nature metabolism

ARTICLES

https://doi.org/10.1038/s42255-018-0025-4

ACC1 determines memory potential of individual CD4$^+$ T cells by regulating de novo fatty acid biosynthesis

Yusuke Endo[1,2], Atsushi Onodera[1], Kazushige Obata-Ninomiya[3], Ryo Koyama-Nasu[1], Hikari K. Asou[1], Toshihiro Ito[1], Takeshi Yamamoto[1], Toshio Kanno[1,2], Takahiro Nakajima[1,2], Kenji Ishiwata[4], Hirotaka Kanuka[4], Damon J. Tumes[1,5] and Toshinori Nakayama[1,6]*

Immunological memory is central to adaptive immunity and protection from disease. Changing metabolic demands as antigen-specific T cells transition from effector to memory cells have been well documented, but the cell-specific pathways and molecules that govern this transition are poorly defined. Here we show that genetic deletion of ACC1, a rate-limiting enzyme in fatty acid biosynthesis, enhances the formation of CD4$^+$ T memory cells. ACC1-deficient effector helper T (Th) cells have similar metabolic signatures to wild-type memory Th cells, and expression of the gene encoding ACC1, *Acaca*, was inversely correlated with a memory gene signature in individual cells. Inhibition of ACC1 function enhances memory T cell formation during parasite infection in mice. Using single-cell analyses we identify a memory precursor–enriched population (CCR7^{hi}CD137^{lo}) present during early differentiation of effector CD4$^+$ T cells. Our data indicate that fatty acid metabolism directs cell fate determination during the generation of memory CD4$^+$ T cells.

Immunological memory is a hallmark of adaptive immunity[1–6], and the quality of adaptive immune responses depends highly on the size of the antigen-specific memory T cell pool[7–10]. In recent years, mounting evidence has shown the importance of cellular metabolism in many aspects of T cell biology[11–18]. Inhibition of mTOR, a critical kinase that regulates cellular metabolism via glycolysis, glutaminolysis and fatty acid biosynthesis, enhances the generation of memory CD8$^+$ T cells[19].

Metabolic profiling has revealed that naive T cells mainly rely on fatty acid oxidation (FAO) as a primary energy source[12,14,15,20]. In contrast, after antigen recognition, T cells reprogram their cellular metabolism to aerobic glycolysis to acquire effector function[12,14,15,20]. Similar to naive T cells, memory T cells use FAO to meet their energy demands[12,14,15,20]. This metabolic switch from glycolysis to FAO is essential for the development and survival of memory CD8$^+$ T cells[12,14,15,20]. Blockade of glycolysis supports memory CD8$^+$ T cell formation, suggesting that graded levels of glycolytic flux in the effector phase can act as a metabolic rheostat to control CD8$^+$ T cell fate determination[21].

Lipid biosynthesis is controlled by sterol regulatory element–binding protein (SREBP), and SREBP expression is increased in activated CD4$^+$ and CD8$^+$ T cells[22]. Increased cholesterol and fatty acid metabolism generates a series of metabolites that are essential for the early activation of T cells[22,23]. Activated T cells or tissue resident T cells take up exogenous fatty acid and cholesterol from their environment[23,24]. Recently, we and other groups have reported that differentiating Th17 cells are highly dependent on the de novo fatty acid synthetic pathway[25–27]. The inhibition of fatty acid biosynthesis either by the pharmacological inhibitor TOFA or using CD4$^+$ T cell–specific ACC1-deficient cells significantly inhibits Th17 cell differentiation and Th17 cell–induced autoimmune disorders[25–27]. These data revealed that de novo fatty acid biosynthesis controls the balance between Th17 cells and regulatory T cells during effector CD4$^+$ Th cell differentiation. However, much less is known about the specific lipid metabolic regulators that control the generation of memory CD4$^+$ T cells.

In the present study, we investigated the role of ACC1 in the generation of memory CD4$^+$ T cells. We found that the genetic deletion or pharmacological inhibition of ACC1 led to increased memory CD4$^+$ T cell formation via alteration of the intrinsic metabolic profiles of effector T cells to resemble those of memory T cells. In individual cells, *Acaca* expression was inversely correlated with the memory gene signature. We also found that early memory precursors were enriched in the CCR7^{hi}CD137^{lo} population. Thus, fatty acid metabolism directs cell fate determination during the generation of memory CD4$^+$ T cells.

Results

ACC1 controls the formation of memory CD4$^+$ T cells. To explore key metabolic pathways that may control the generation of functional memory CD4$^+$ T cells, we began by comparing gene expression profiles of naive CD4$^+$ T cells, effector Th cells and memory CD4$^+$ T cells (Supplementary Fig. 1). The expression of *Acaca*, which encodes ACC1, a rate-limiting enzyme for fatty acid biosynthesis, and that of several other genes associated with fatty acid biosynthesis was increased in effector Th cells and decreased in memory CD4$^+$ T cells (Supplementary Fig. 1a). Memory Th1 cells generated in our study expressed a substantial proportion of the genes previously identified as CD8$^+$ T cell memory signature genes; these included *Il7r*, *Klf2*, *Tcf7*, *Irf7*, *Foxp1* and *Foxo1*

[1]Department of Immunology, Graduate School of Medicine, Chiba University, Chuo-ku, Chiba, Japan. [2]Laboratory of Medical Omics Research, KAZUSA DNA Research Institute, Kisarazu, Chiba, Japan. [3]Department of Advanced Allergology of the Airway, Graduate School of Medicine, Chiba University, Chuo-ku, Chiba, Japan. [4]Department of Tropical Medicine, The Jikei University School of Medicine, Tokyo, Japan. [5]Centre for Cancer Biology, University of South Australia and SA Pathology, Adelaide, SA, Australia. [6]AMED-CREST, AMED, Chuo-ku, Chiba, Japan. *e-mail: tnakayama@faculty.chiba-u.jp

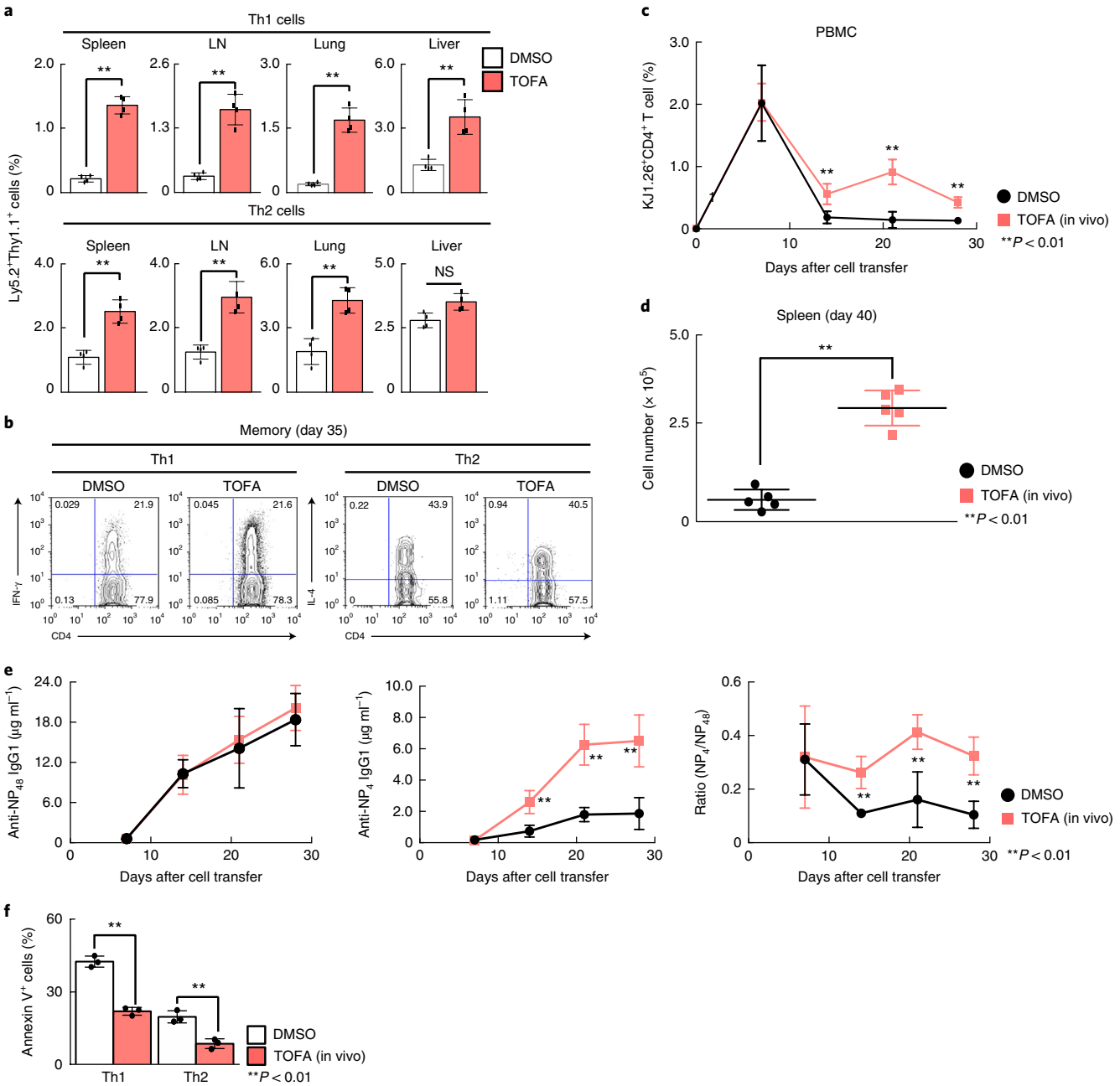

Fig. 1 | Pharmacological inhibition of ACC1 function enhances the formation of antigen-specific memory CD4+ T cells. a, TOFA-treated effector Th1 or Th2 cells expressing the DO11.10 TCR were intravenously transferred into syngeneic BALB/c mice. Memory Th1 or Th2 cells were generated in vivo 4–5 weeks after cell transfer as in Supplementary Fig. 2a. Proportions of KJ1$^+$ memory Th1 and Th2 cells in the spleen, lymph node (LN), lung and liver was determined by flow cytometry (DMSO, $n=4$; TOFA, $n=4$ biologically independent samples). NS, not significant. **b**, Intracellular staining profiles of IFN-γ and IL-4 in PMA and ionomyin-stimulated memory Th1 or Th2 cells, respectively. Flow cytometry gates for positive or negative IFN-γ and IL-4 expression were determined by staining without re-stimulation. **c**, Naive CD4$^+$ T cells (5×10^5) from DO11.10 TCR transgenic mice were transferred into naive BALB/c mice. Kinetics of ovalbumin-specific KJ1$^+$CD4$^+$ T cells in PBMCs of ovalbumin-immunized BALB/c mice treated with TOFA (from day −1 to day 4 post-immunization) or DMSO (DMSO, $n=5$; TOFA, $n=6$ biologically independent samples). **d**, Ovalbumin-specific memory CD4$^+$ T cells (day 40 post-immunization) were generated in vivo in the presence of TOFA. Cell number of KJ1$^+$ memory CD4$^+$ T cells in spleen was determined by flow cytometry (DMSO, $n=5$; TOFA, $n=5$ biologically independent samples). **e**, TOFA treatment enhances production of high-affinity antibodies in vivo. Naive CD4 T cells from DO11.10 TCR transgenic mice were transferred into naïve BALB/c mice, and the mice were then immunized i.p. with 100 μg NP-ovalbumin plus alum. Ovalbumin-immunized BALB/c mice were treated with TOFA (from day −1 to day 4 post-immunization) or DMSO (DMSO, $n=6$; TOFA, $n=6$ biologically independent samples). Blood samples taken at each time point were analyzed for anti-NP_{48}-IgG1 and anti-NP_4-IgG1 by enzyme-linked immunosorbent assay (ELISA). **f**, Susceptibility to apoptosis of effector Th1 or Th2 cells treated with or without TOFA was investigated by annexin V and PI staining ($n=3$ per each group biologically independent samples). $^{**}P<0.01$, $^{*}P<0.05$ (one-way analysis of variance (ANOVA) with Mann-Whitney *U*-test (**a**,**f**) or two-tailed Student's *t*-test (**c**–**e**)). Each symbol (**a**,**d**,**f**) represents an individual mouse; the measure of center (**a**,**c**–**f**) indicates mean ± s.e.m (**a**,**c**,**d**) or s.d. (**e**,**f**). Three technical replicates were performed for ELISA (**e**). Three independent experiments were performed with similar results for **a**–**e**. Five independent experiments were performed with similar results for **f**.

(Supplementary Fig. 1b)[28]. Gene set enrichment analysis revealed significantly decreased transcription of genes involved in the fatty acid biosynthesis pathway in memory T cells when compared to effector cells (Supplementary Fig. 1c). Recently, we and other groups have reported that differentiating Th17 cells are highly dependent on the de novo fatty acid synthetic pathway using *Acaca*$^{-/-}$ mice[25–27]. In the present study, we define a new function for ACC1 as a regulator of the CD4$^+$ T cell effector-memory fate decision. We first treated ovalbumin-specific differentiating Th1 and Th2 cells in vitro with TOFA, an allosteric inhibitor of ACC1, and then transferred these cells into syngeneic recipient mice to monitor antigen-specific Th1 and Th2 cells persisting in vivo (Supplementary Fig. 2a). TOFA had no effect on the differentiation of effector Th1 and Th2 cells, as has been reported previously[25] (Supplementary Fig. 2b). However, TOFA treatment in vitro significantly increased the proportion and number of antigen-specific memory Th1 and Th2 cells in the spleen, lymph node, lung and liver (Fig. 1a and Supplementary Fig. 2c–f). Enhanced generation of memory Th1 cells in TOFA-treated cells was seen 1 week after cell transfer and persisted for >4 weeks (Supplementary Fig. 2e). Similar cytokine production profiles were observed for interferon-γ (IFN-γ) and interleukin-4 (IL-4) in the TOFA-treated groups, indicating that TOFA does not alter the functional polarization of memory CD4$^+$ T cells (Fig. 1b).

We next examined the effect of in vivo administration of TOFA on memory CD4$^+$ T cell generation (Supplementary Fig. 3a). Ovalbumin-specific T-cell receptor (TCR)-transgenic naive CD4$^+$ T cells were intravenously transferred into syngeneic mice. These mice were then injected with ovalbumin adsorbed to alum, followed by intraperitoneal (i.p.) administration of TOFA (1 mg kg^{-1}) or the solvent dimethylsulfoxide (DMSO) as a control. Similar proportions of ovalbumin-specific effector CD4$^+$ T cells were observed in the control and TOFA-treated groups with a peak on day 5 after immunization; however, mice from the TOFA-treated group showed significantly less contraction of this population compared to the control group (Fig. 1c). The number of ovalbumin-specific CD4$^+$ T cells was significantly higher in the TOFA-treated group than in the control group at 40 days after initial antigen exposure (Fig. 1d and Supplementary Fig. 3). Furthermore, TOFA administration led to significantly higher (4-hydroxy-3-nitrophenyl)acetyl (NP)-specific high-affinity (Fig. 1e, center and right), but not low-affinity, antibody 28 days after immunization with NP-coupled ovalbumin plus alum (Fig. 1e, left), whereas on day 7, the levels of high-affinity and low-affinity IgG1 were comparable (Fig. 1e). Owing to the strong effects of TOFA on the formation of antigen-specific memory Th cells, the enhancement in high-affinity antibody production is probably due to increased help from antigen-specific Th cells. To investigate the mechanism underlying ACC1-mediated control of memory CD4$^+$ T cell generation, we assessed apoptotic cell death of in vitro–differentiated Th1 and Th2 cells by measuring the number of annexin V$^+$ and propidium iodide (PI)$^+$ cells after 1-day culture without cytokines. TOFA-treated Th1 and Th2 cells showed significantly decreased apoptosis compared to control cells (Fig. 1f and Supplementary Fig. 7a,b). Similarly, TOFA treatment showed decreased apoptosis of human Th1 and Th2 cells (Supplementary Fig. 7e). Notably, TOFA treatment did not inhibit apoptotic cell death of Th17 cells or CD8$^+$ T cells (Supplementary Fig. 7f,g), consistent with a previous study using *Acaca*$^{-/-}$ CD8$^+$ T cells[29].

We then analyzed the effect of ACC1 on the generation of memory CD4$^+$ T cells using inducible ERT2-*Acaca*-deficient mice[30] (Supplementary Fig. 4a,b). ACC1-mediated fatty acid biosynthesis is required for early activation and proliferation of T cells[23]. Therefore, to avoid effects of ACC1 deficiency during initial activation of T cells, we added 4-hydroxy tamoxifen (4-OHT) into the in vitro culture from day 2 to day 5 to delete *Acaca* for analysis of the generation of memory CD4$^+$ T cells. Th1 and Th2 cell differentiation was unaffected by genetic deletion of *Acaca* (Supplementary Fig. 4c). Both the proportion and number of memory Th1 and Th2 cells were significantly increased in ERT2-cre$^+$*Acaca*$^{fl/fl}$ (*Acaca*$^{-/-}$) groups as compared to *Acaca*$^{+/+}$ groups, as noted in the TOFA-treatment experiments (Fig. 2a and Supplementary Fig. 4d). We also confirmed similar cytokine production profiles of IFN-γ and IL-4 in Th1 and Th2 cells, respectively, in the absence of ACC1 (Fig. 2b). Furthermore, we examined the effect of *Acaca* deletion on the formation of memory CD4$^+$ T cells using an ovalbumin immunization system (Fig. 2c and Supplementary Fig. 5a,b). Ovalbumin-specific CD4$^+$ T cells preferentially use the Vα2$^+$ T cell receptor[31]. To analyse polyclonal ovalbumin specific T cells, we therefore analysed Vα2$^+$CD4$^+$ T cells that expressed the activation and memory marker CD44 and were negative for the regulatory T cell marker Foxp3 (Vα2$^+$CD44^{hi}Foxp3$^-$CD4$^+$ T cells). We observed that the number of Vα2$^+$ memory CD4$^+$ T cells was

Fig. 2 | Genetic deletion of ACC1 enhances formation of antigen-specific memory CD4+ T cells. a, Ly5.1$^+$ effector Th1 or Th2 cells were differentiated from ERT2-cre$^+$ *Acaca*$^{+/+}$ or ERT2-cre$^+$ *Acaca*$^{fl/fl}$ mice-derived naive CD4$^+$ T cells in the presence of 4-OHT (100 nM, days 2–5) and intravenously transferred into syngeneic B6 mice. *Acaca*$^{+/+}$- or *Acaca*$^{-/-}$-memory Th1 or Th2 cells were generated in vivo 4–5 weeks after the cell transfer. Summary data for the memory Th1/Th2 cell population (Ly5.1 and CD4) in splenocytes from mice receiving *Acaca*$^{+/+}$- or *Acaca*$^{-/-}$-effector Th1 or Th2 cells (*Acaca*$^{+/+}$, $n=5$; *Acaca*$^{-/-}$, $n=5$ biologically independent samples). **b**, Intracellular staining profiles of IFN-γ for Th1 and IL-4 for Th2 in *Acaca*$^{+/+}$- or *Acaca*$^{-/-}$-memory Th1 or Th2 cells. IFN-γ-positive or negative or IL-4-positive or negative cells were determined by the staining of these cells without re-stimulation with PMA plus ionomycin. **c**, Naive CD4$^+$ T cells from ERT2-Cre$^+$*Acaca*$^{+/+}$- or ERT2-Cre$^+$*Acaca*$^{fl/fl}$-Ly5.1$^+$OT II transgenic mice were transferred into naive C57BL/6 mice. Ovalbumin-specific memory CD4$^+$ T cells (day 40 post-immunization) were generated in vivo in the presence of tamoxifen (from day 2 to day 6). On day 40, these mice were challenged with ovalbumin for analysis of re-expansion. The proportion and number of donor-derived Ly5.1$^+$ memory CD4$^+$ T cells in the lung was determined by flow cytometry (*Acaca*$^{+/+}$, $n=4$; *Acaca*$^{-/-}$, $n=4$ biologically independent samples). **d**, CD4-Cre$^+$*Acaca*$^{+/+}$ or CD4-Cre$^+$*Acaca*$^{fl/fl}$ mice were immunized with ovalbumin-alum, and these mice were challenged with ovalbumin on day 40. The number of CD44^{hi}Vα2$^+$Foxp3$^-$CD4$^+$ T cells in the lung was determined by flow cytometry (*Acaca*$^{+/+}$, $n=5$; *Acaca*$^{-/-}$, $n=5$ biologically independent samples). **e**, Intracellular staining profiles of IL-4 in *Acaca*$^{+/+}$- or *Acaca*$^{-/-}$-CD44^{hi}Vα2$^+$Foxp3$^-$CD4$^+$ T cells (*Acaca*$^{+/+}$, $n=5$; *Acaca*$^{-/-}$, $n=5$ biologically independent samples). **f**, *Acaca*$^{+/+}$ (Ly5.1$^+$Ly5.2$^-$) or *Acaca*$^{fl/fl}$ (Ly5.1$^+$Ly5.2$^+$) naive CD4$^+$ T cells were transferred into normal recipient mice, and these mice were infected with Nb with the administration of tamoxifen (from day 10 to day 14). On day 40, these mice were re-infected with Nb for analysis of recall responses. The proportion and number of donor-derived memory CD4$^+$ T cells in the spleen and lung were determined by flow cytometry (*Acaca*$^{+/+}$, $n=5$; *Acaca*$^{-/-}$, $n=5$ biologically independent samples). **g**, Intracellular staining profiles of IFN-γ and IL-4 for helminth-induced *Acaca*$^{+/+}$- or *Acaca*$^{-/-}$-memory CD4$^+$ T cells (*Acaca*$^{+/+}$, $n=5$; *Acaca*$^{-/-}$, $n=5$ biologically independent samples). **h**, Absolute number of worms in small intestine on day 7 after subcutaneous inoculation of 2,000 Nb L3. **i**, Susceptibility to apoptosis of *Acaca*$^{+/+}$- or *Acaca*$^{-/-}$-effector Th1 or Th2 cells was investigated by annexin V and PI staining ($n=4$ biologically independent samples per group). **j**, Susceptibility to apoptosis of *Acaca*$^{+/+}$- or *Acaca*$^{-/-}$-effector Th1 or Th2 cells was investigated ex vivo (48 h after cell transfer into syngeneic B6 mice; $n=4$ biologically independent samples per each group). $^{**}P<0.01$, $^{*}P<0.05$ (one-way ANOVA with Mann-Whitney *U*-test (**i**,**j**) or two-tailed Student's *t*-test (**a**,**c**–**h**)). Each symbol (**a**,**c**–**h**) represents an individual mouse; the measure of center (**a**,**c**–**j**) indicates mean ± s.e.m. (**a**,**c**–**h**) or s.d. (**i**,**j**). Three independent experiments were performed with similar results for **a**,**b**. Five independent experiments were performed with similar results for **i**. Two independent experiments were performed with similar results for **c**–**h**,**j**.

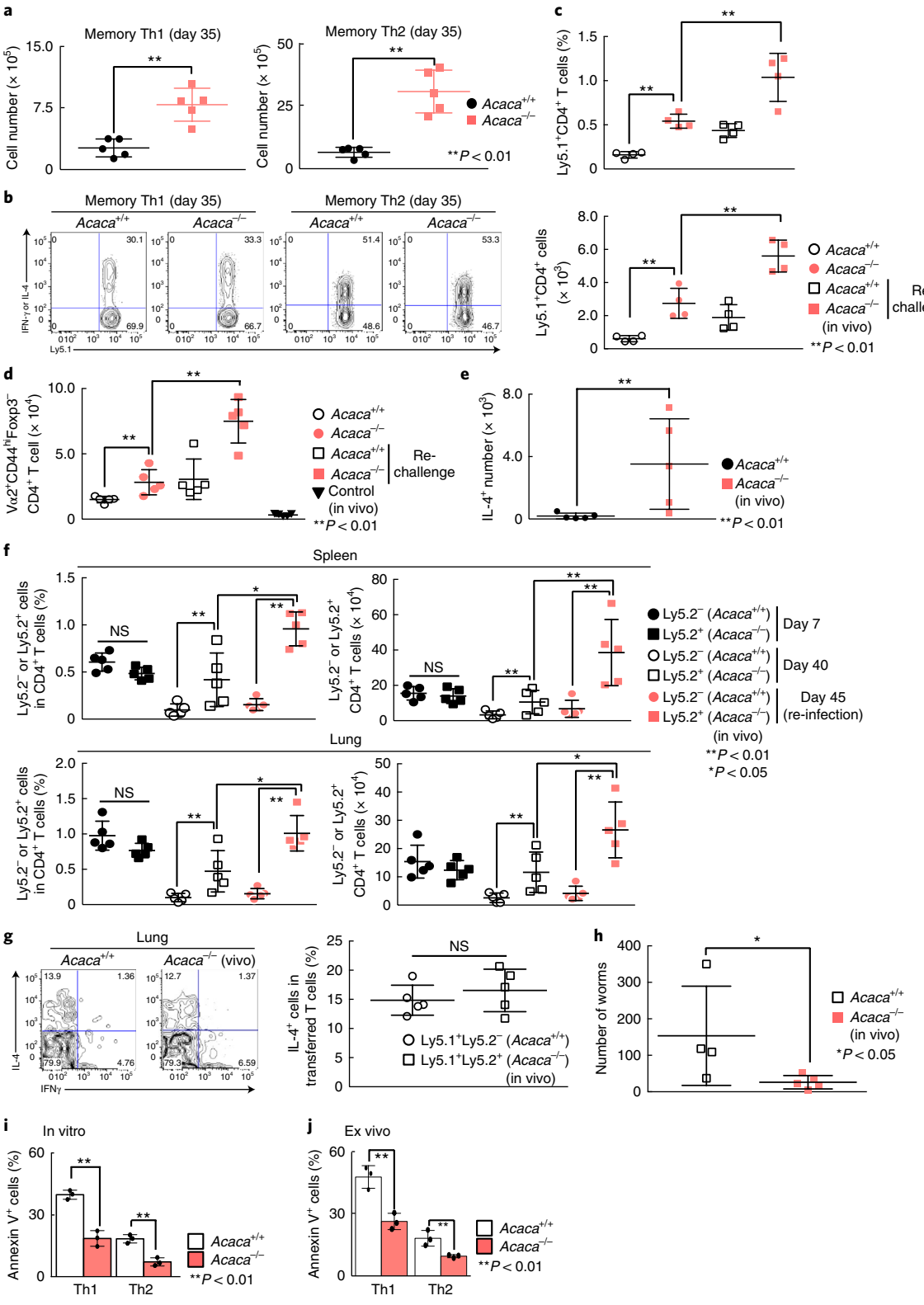

significantly higher in the *Acaca*$^{-/-}$ group than in the *Acaca*$^{+/+}$ group without adoptive transfer (Fig. 2d and Supplementary Fig. 5c,d). IL-4-producing Vα2^{+} memory CD4^{+} T cells were also increased in the *Acaca*$^{-/-}$ group in this system (Fig. 2e).

To address ACC1-regulated memory CD4^{+} T cell generation and function in an infection model, we examined T cell–specific ablation of ACC1 in a helminth infection model (Supplementary Fig. 6a). A significantly greater proportion and number of memory CD4^{+} T cells were detected in the *Acaca*$^{-/-}$ group (Ly5.1^{+}Ly5.2^{+}) as compared to the *Acaca*$^{+/+}$ group (Ly5.1^{+}Ly5.2^{-}) (Fig. 2f). We also observed increased numbers of PD1^{+}CXCR5^{+} follicular helper T cells in the *Acaca*$^{-/-}$ group (Supplementary Fig. 6b–d). Consistent with these results, GL-7^{+}Fas^{+} markers for germinal center B cells were increased in the *Acaca*$^{-/-}$ group (Supplementary Fig. 6e–g). We also confirmed that equivalent proportions of *Acaca*$^{-/-}$ CD4^{+} T cells produced IL-4 upon reinfection with *Nippostrongylus brasiliensis* (Nb)

(Fig. 2g). Furthermore, we examined the effect of *Acaca* deletion on memory T cell-mediated protection against Nb infection without adoptive T cell transfer (Supplementary Fig. 6h). Numbers of Nb worms in the intestine of *Acaca*$^{-/-}$ mice 7 days after secondary inoculation with Nb were lower than those in wild-type mice (Fig. 2h). These results show that both genetic deletion and functional inhibition of ACC1 enhances the formation of antigen-specific memory CD4$^+$ T cells while leaving their ability to produce signature cytokines intact. Similar to the results obtained from TOFA treatment, *Acaca*-deficient Th1 and Th2 cells showed significantly decreased apoptosis compared to control cells in in vitro and ex vivo experimental systems (Fig. 2i,j and Supplementary Fig. 7c,d). Inhibition of glycolysis by treatment with 3-bromopyruvate[32], a pharmacological inhibitor of hexokinase 2, did not affect apoptotic cell death of Th1 or Th2 cells (Supplementary Fig. 7h). Thus, fatty acid biosynthesis in effector Th1 and Th2 cells may have a critical influence on their formation of memory Th1 and Th2 cells via regulation of cell survival.

ACC1 controls cellular metabolites associated with TCA cycle. Metabolome analysis was next carried out to determine how ACC1 influences the metabolic profiles of both effector and memory CD4$^+$ T cells. We found that almost all metabolites associated with the tricarboxylic acid (TCA) cycle were increased in TOFA-treated effector Th1 cells compared to control cells (DMSO-treated group) (Fig. 3a and Supplementary Fig. 8a). A group treated with the mTOR inhibitor rapamycin was included as a positive control, and as we expected, similarly enhanced levels of TCA-cycle-associated metabolites were induced. Ratios of NADPH/NADP$^+$, GSH/GSSG, and AMP/ATP, indicators of a cellular redox state and susceptibility to apoptosis, were also all increased in TOFA-treated effector Th1 cells compared to control cells (Fig. 3b). In contrast, the levels of glycolysis-associated metabolites, such as glucose-6p, fructose-6p or phosphoenolpyruvate, were decreased by TOFA treatment (Supplementary Fig. 8b). Similarly increased levels of TCA-cycle-associated metabolites and ratios of NADPH/NADP$^+$, GSH/GSSG and AMP/ATP were also observed in *Acaca*-deficient effector Th1 cells (Fig. 3c,d and Supplementary Fig. 8c). Moreover, increased levels of TCA cycle–associated metabolites were detected in memory Th1 cells that were very similar to *Acaca*-deficient effector Th1 cells (Fig. 3c,d). These results indicate that inhibition of ACC1-mediated fatty acid biosynthesis alters the metabolic profile of effector T cells to resemble that of memory T cells.

We next directly assessed mitochondrial function and rate of acid efflux in TOFA-treated or *Acaca*-deficient CD4$^+$ T cells by monitoring the oxygen consumption rate (OCR) and extracellular acidification rate in response to sequential treatment with the ATPase inhibitor oligomycin, the uncoupling agent carbonyl cyanide 4-(trifuluoromethoxy)phenylhydrazone (FCCP), and the electron-transport-chain inhibitors rotenone and antimycin A. TOFA-treated or *Acaca*-deficient effector Th1 or Th2 cells demonstrated significantly more mitochondrial spare respiratory capacity (SRC) than control cells (Fig. 3e,f and Supplementary Fig. 8f), consistent with the increased TCA cycle–associated metabolites identified in the metabolome analysis (Fig. 3a,c). Conversely, the level of extracellular acidification rate was decreased in TOFA-treated or *Acaca*-deficient effector Th1 and Th2 cells, again consistent with the levels of glycolysis-associated metabolites (Supplementary Fig. 8d,e,g). In addition, TOFA-treated human Th1 cells showed significantly more mitochondrial SRC than control cells (Supplementary Fig. 8h,i). Therefore, TOFA-treated and *Acaca*-deficient effector Th cells have a metabolic phenotype closely resembling memory Th cells that is accompanied by increased mitochondrial activity.

ACC1 controls anti-apoptotic program via regulation of FAO. To analyze the interrelationship between enhanced memory cell formation and cellular metabolic changes in *Acaca*$^{-/-}$ Th cells, we first examined the expression of anti-apoptotic genes including *Bcl2*, *Bcl211* and *Mcl1*. Consistent with longevity, these factors were enriched in TOFA-treated- or *Acaca*$^{-/-}$ Th1 and Th2 cells (Fig. 4a and Supplementary Fig. 9a). The longevity of memory T cells requires programs to reduce oxidative stress[33]. We therefore tested intrinsic oxidative stress levels, mitochondrial mass, and mitochondrial membrane potential in these cells. The deficiency of ACC1 in Th cells led to reduced reactive oxygen species (ROS) levels as measured by CellRox, a novel fluorogenic ROS probe (Fig. 4b). *Acaca*$^{-/-}$ Th cells also showed decreased mitochondrial membrane potential by tetramethylrhodamine, ethyl ester (TMRE) staining without affecting mitochondrial mass (Fig. 4b). Furthermore, these cells had reduced levels of DNA damage, as assayed by Ser139 phosphorylated histone variant H2A.X (Fig. 4c). In addition, mRNA expression of ROS-detoxifying enzymes including superoxide dismutase 1 and superoxide dismutase 2 (encoded by *Sod1* and *Sod2*, respectively) was increased in *Acaca*$^{-/-}$ Th cells (Supplementary Fig. 9b). A series of experiments demonstrated that *Acaca*$^{-/-}$ Th cells are more resistant to oxidative stress and ROS-induced DNA damage, which may predispose these cells to longevity. *Acaca*$^{-/-}$ Th cells also displayed increased levels of carnitine palmitoyl transferase 1a (encoded by *Cpt1a*), the rate-limiting enzyme associated with transport of fatty acid into the mitochondria for subsequent β-oxidation (Fig. 4d). Recent findings have revealed a strong link between FAO and T cell longevity[34]. To determine whether the enhanced SRC and longevity in *Acaca*$^{-/-}$ Th cells depends on FAO, we cultured these cells under glucose-free or fatty acid–free conditions. In fatty acid–free conditions, apoptosis of *Acaca*-deficient Th cells was increased to levels similar to those in *Acaca*$^{+/+}$ Th cells (Fig. 4e and Supplementary Fig. 9c). Similar results were detected for *Acaca*$^{-/-}$ Th cells treated with the Cpt1 inhibitor etomoxir (Fig. 4f and Supplementary Fig. 9d). Furthermore, extracellular fatty acid deprivation impaired SRC in *Acaca*-deficient Th cells and returned SRC to levels similar to those in *Acaca*$^{+/+}$ cells (Fig. 4g). The generation of memory Th1 cells from *Acaca*$^{-/-}$ effector Th1 cells cultured under fatty acid-free conditions was also impaired (Fig. 4h). Together, our data suggest that *Acaca*-deficient Th cells use the FAO program, which enables these cells to establish long-term persistence in vivo.

Fig. 3 | ACC1 controls intracellular metabolites associated with TCA cycle and mitochondrial respiration in early-differentiating effector CD4$^+$ T cells. **a**, Metabolome analysis of effector Th1 cells treated with rapamycin (Rap.), TOFA or DMSO. Value for each metabolite represents average of triplicates. α-KG, α-ketoglutaric acid. **b**, Ratio of NADPH/NADP$^+$, GSH/GSSG and AMP/ATP in effector Th1 (eTh1) cells treated with rapamycin, TOFA or DMSO. **c**, Metabolome analysis of *Acaca*$^{+/+}$- or *Acaca*$^{-/-}$-effector Th1 cells and memory Th1 (mTh1) cells. OAA, oxaloacetic acid. **d**, Ratio of NADPH/NADP$^+$, GSH/GSSG or AMP/ATP in *Acaca*$^{+/+}$- or *Acaca*$^{-/-}$-effector Th1 cells and memory Th1 cells. Value for each metabolite represents average of triplicates. **e**, OCR of effector Th1 cells treated with or without TOFA under basal conditions (time point 0) and in response to sequential treatment with oligomycin, FCCP and rotenone-antimycin A (DMSO, $n=5$; TOFA, $n=5$ biologically independent samples). **f**, OCR of *Acaca*$^{+/+}$- or *Acaca*$^{-/-}$-effector Th1 cells under basal conditions (time point 0) and in response to sequential treatment with oligomycin, FCCP and rotenone-antimycin A (*Acaca*$^{+/+}$, $n=5$; *Acaca*$^{-/-}$, $n=5$ biologically independent samples). $^{**}P<0.01$, $^{*}P<0.05$ (one-way ANOVA with Mann-Whitney *U*-test (**a**–**d**) or two-tailed Student's *t*-test (**e**,**f**)). Each symbol (**a**–**d**) represents an individual mouse; the measure of center (**a**–**f**) indicates mean ± s.e.m. Three biological replicates were performed for metabolome analysis (**a**–**d**). Four biological replicates were performed for seahorse analysis (**e**,**f**). Two independent experiments were performed with similar results for **e**,**f**.

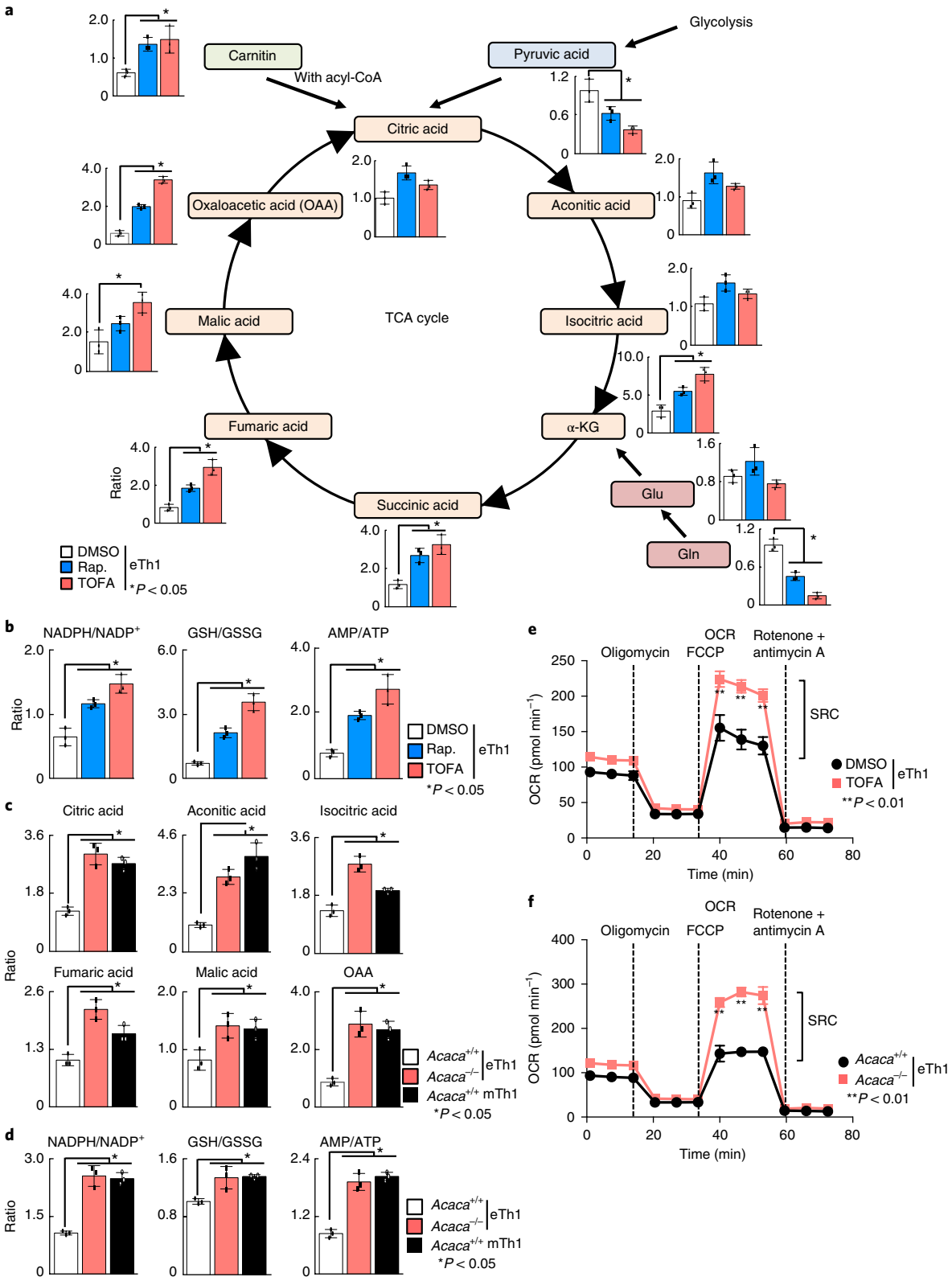

Acaca-controlled genes predicts memory CD4⁺ T cell fates. We hypothesized that ACC1 might repress a genetic program that confers specialization from effector to memory T cells. To characterize the genetic profiles of memory T cells and assess the influence of ACC1 expression on the memory T cell genetic signature, we used a combination of genome-wide and single-cell gene-expression profiling. We first did microarray analysis to identify memory-specific and also ACC1-controlled genes in naive CD4⁺ T, effector Th1, TOFA-treated effector Th1, memory Th1 and memory Th2 cells. A schematic representation of the method used to select candidate genes is in Supplementary Fig. 10a. Focusing on the fatty acid biosynthesis program, we selected 96 of the 147 candidate genes for single-cell gene-expression profiling (Supplementary Fig. 10b). These genes encode regulators of apoptosis, metabolic enzymes,

transcription factors, cytokines and cytokine receptors, cell surface molecules, and signaling molecules (Supplementary Fig. 10b). Expression of 15 of these genes in naive CD4+ T cells, effector Th1 and memory Th1 cells was confirmed by quantitative real-time polymerase chain reaction (quantitative rtPCR) (Supplementary Fig. 11). Fluidigm 96.96 Dynamic Arrays were then used to perform simultaneous quantitative rtPCR measurement of the expression of the 96 selected genes in 96 individual cells[35,36] isolated from populations of naive CD4+ T cells, effector Th1 cells and memory Th1 cells. We used principal component analysis (PCA) to visualize the gene expression pattern in each T cell population. The PCA revealed that effector Th1 cells formed a cluster distinct from naive CD4+ T cells and memory Th1 cells (Supplementary Fig. 12a). Notably, PCA of a set of seven genes related to fatty acid biosynthesis demonstrated that a proportion of the effector Th1 cells were positioned away from the bulk of the effector Th1 cells and were more similar to memory Th1 cells (indicated by dotted line box in Supplementary Fig. 12b, left panel). This separation of the effector Th1 subset was not evident when six genes related to glycolysis were analyzed by PCA (Supplementary Fig. 12b, right panel). Violin plots of expression of individual genes in each cell revealed that effector Th1 cells were clearly divided into two populations based on expression of the fatty acid biosynthetic genes *Acaca*, *Acsl3*, *Fads2* and *Mcat* (Fig. 5a). These two subpopulations could not be resolved by analysis of bulk populations of effector Th1 cells (Supplementary Fig. 12c). In contrast to the fatty acid biosynthetic genes, glycolytic genes seem to show a more homogeneous expression pattern in effector Th1 cells (Fig. 5b). Similar observations were made using single-cell analysis of effector Th2 cells (Supplementary Fig. 12d–g). These results led us to postulate that expression of *Acaca* might distinguish effector lineage cells from memory lineage cells at the early stages of differentiation from naive to effector Th1 and Th2 cells.

Statistical analysis using a chi-squared test based on the expression of *Acaca* in single cells showed that expression of *Acaca* was negatively correlated with that of memory signature genes *Klf2*, *Ccr7*, *Tcf7*, *Irf7*, *Gpr34* and *Foxo1* and was positively correlated with expression of *Ltb4r1*, *Fads2*, *Tnfrsf9*, *Hsd17b7*, *Caspase9*, *Acsl3*, *Mcat* and *Hmgcs1* in both effector Th1 and Th2 cells (see shared genes in Fig. 5c and Supplementary Fig. 12h). *Klf2*, *Ccr7* and *Tcf7* are associated with the memory cell population, and *Caspase9* and fatty acid biosynthetic enzymes are strongly induced in effector cells[1]. We also visualized the relationship between expression of *Acaca* and other genes in single CD4+ T cells at different stages of differentiation (*Acaca*^{hi}-, *Acaca*^{lo}-, TOFA-treated- and *Acaca*$^{-/-}$-effector Th1 and Th2 and memory Th1 and Th2 cells) using PCA, violin plots and heat map analysis (Fig. 5d–f and Supplementary Fig. 12i). PCA of the genes that were expressed in concert with *Acaca* in *Acaca*^{hi}-, *Acaca*^{lo}- and *Acaca*$^{-/-}$-effector Th1 cells and memory Th1 cells showed that *Acaca*^{lo}- and *Acaca*$^{-/-}$-effector Th1 cells tended to more closely resemble memory Th1 cells than *Acaca*^{hi}-effector cells (Fig. 5d). Several of the genes whose expression was negatively correlated with the expression of *Acaca* (*Ccr7*, *Tcf7* and *Gpr34*) were more highly expressed in *Acaca*^{lo}-, TOFA-treated- and *Acaca*$^{-/-}$-effector Th1 cells and memory Th1 cells at the single-cell level as compared to their expression in *Acaca*^{lo}-Th1 cells (Fig. 5e). In contrast, genes whose expression was positively correlated with that of *Acaca* (*Tnfrsf9*, *Caspase9*, *Gipr* and *Emilin2*) showed a similar expression pattern to that of *Acaca* and were expressed less in single *Acaca*^{lo}-, TOFA-treated- and *Acaca*$^{-/-}$-effector Th1 and memory Th1 cells. Heatmap analysis showed that the expression of *Klf2*, *Ccr7*, *Tcf7*, *Irf7* and *Gpr34* was higher in single *Acaca*^{lo}- and *Acaca*$^{-/-}$-effector Th1 and Th2 cells and single memory Th1 and Th2 cells compared to single *Acaca*^{hi}-effector Th1 and Th2 cells (Fig. 5f,g and Supplementary Fig. 12i). In contrast, the expression of *Ltb4r1*, *Tnfrsf9*, *Caspase9* and *Gipr* was lower in *Acaca*^{lo}- and *Acaca*$^{-/-}$-effector and memory Th1 cells at the single-cell level (Fig. 5f,g). A similar pattern for *Caspase9*, *Ltb4r1*, *Tnfrsf9* and *CCR4* was detected in Th2 cells (Supplementary Fig. 12i). Thus, *Acaca*^{lo} effector Th1 and Th2 cells show preferential expression of memory-signature genes. These results indicate that the absence of *Acaca* upregulation during early effector Th cell may be characteristic of progenitor cells with memory T cell potential.

CCR7 and CD137 define memory T precursor–enriched population. Whether it is possible to define separate lineages of memory and effector T cells during the early stages of an immune response is a major unanswered question in immunology. We next sought to determine whether we could use our single-cell gene-expression analysis to identify surface markers that can distinguish effector and memory cell lineages during the early stages of differentiation from naive CD4+ T cells into effector Th cells. Our single-cell gene expression profiling showed that expression of CD137 (gene product of *Tnfrsf9*) was closely correlated with *Acaca* expression, and that *CCR7* was inversely correlated with *Acaca* expression. *Tnfrsf9* was also detected in the gene set that is downregulated in memory T cells (Supplementary Fig. 1b). These cell surface molecules may therefore distinguish memory precursor and short-lived effector cell fates, and thus we examined the expression of CCR7 and CD137 in antigen-specific CD4+ T cells at various stages of differentiation (naive, early-differentiating effector and memory) (Supplementary Fig. 13a). Antigen-specific naive and memory CD4+ T cells showed a CCR7^{hi}CD137^{lo} phenotype, whereas the majority of early-differentiating effector cells displayed a CCR7^{lo}CD137^{hi} phenotype (Fig. 6a). TOFA-treated effector Th1 or Th2 cells and human Th1 or Th2 cells showed an increase in the CCR7^{hi}CD137^{lo} population (Fig. 6b and Supplementary Figs. 13b and 14a). Similarly, genetic deletion of *Acaca* enhanced the proportion of CCR7^{hi}CD137^{lo} cells (Fig. 6c and

Fig. 4 | ACC1 controls anti-apoptotic program via regulation of fatty acid oxidation in early-differentiating effector CD4+ T cells. a, Quantitative rtPCR analysis of anti-apoptotic genes including *Bcl2* and *Bclxl* in TOFA-treated-*Acaca*$^{+/+}$- or *Acaca*$^{-/-}$-effector Th1 and Th2 cells. **b**, Oxidative stress levels (CellRox), mitochondrial mass (Mitotracker) and mitochondrial membrane potential (TMRE) in *Acaca*$^{+/+}$- or *Acaca*$^{-/-}$-effector Th1 and Th2 cells. Summary data of relative mean fluorescence intensity (MFI) of TMRE and CellRox is in lower panels. (*Acaca*$^{+/+}$, $n=3$; *Acaca*$^{-/-}$, $n=3$ biologically independent samples). **c**, Phosphorylated histone variant H2A.X (pH2AX) in *Acaca*$^{+/+}$- or *Acaca*$^{-/-}$-effector Th1 and Th2 cells. **d**, Quantitative rtPCR analysis of *Cpt1a* in TOFA-treated-*Acaca*$^{+/+}$- or *Acaca*$^{-/-}$-effector Th1 and Th2 cells. **e**, Apoptosis of *Acaca*$^{+/+}$- or *Acaca*$^{-/-}$-effector Th1 cells cultured with control, glucose-free or fatty acid (FA)-free medium was investigated ($n=4$ biologically independent samples per each group). **f**, Apoptosis of *Acaca*$^{+/+}$- or *Acaca*$^{-/-}$-effector Th1 cells in presence or absence of etomoxir was investigated by annexin V and PI staining ($n=4$ biologically independent samples per each group). **g**, OCR of *Acaca*$^{+/+}$- or *Acaca*$^{-/-}$-effector Th1 cells cultured in control or fatty acid–free medium ($n=4$ biologically independent samples per each group). **h**, Memory Th1 cell population (Ly5.1 and CD4) in splenocytes from mice receiving *Acaca*$^{+/+}$- or *Acaca*$^{-/-}$-effector Th1 cells cultured in control or fatty acid–free medium (*Acaca*$^{+/+}$, $n=4$; *Acaca*$^{-/-}$ control medium, $n=4$; *Acaca*$^{-/-}$ fatty acid–free medium, $n=4$ biologically independent samples). Mean values with s.e.m. are shown for **a**–**g**,**j**–**m**. Mean values with s.d. are shown for **b**,**h**. $^{**}P<0.01$, $^{*}P<0.05$ (one-way ANOVA with Mann-Whitney *U*-test (**i**,**j**), or two-tailed Student's *t*-test (**a**,**c**–**h**)). Each symbol (**a**,**c**–**h**) represents an individual mouse; the measure of center (**a**,**c**–**j**) indicates mean ± s.e.m. (**h**) or s.d. (**a**,**b**,**d**–**g**)). Four biological replicates were performed for seahorse analysis (**g**). Three technical replicates and four biological replicates were performed for quantitative rtPCR analysis (**a**,**d**). Two independent experiments were performed with similar results for **b**,**c**,**g**,**h**. Three (**e**,**f**) and four (**a**,**d**) independent experiments were performed with similar results.

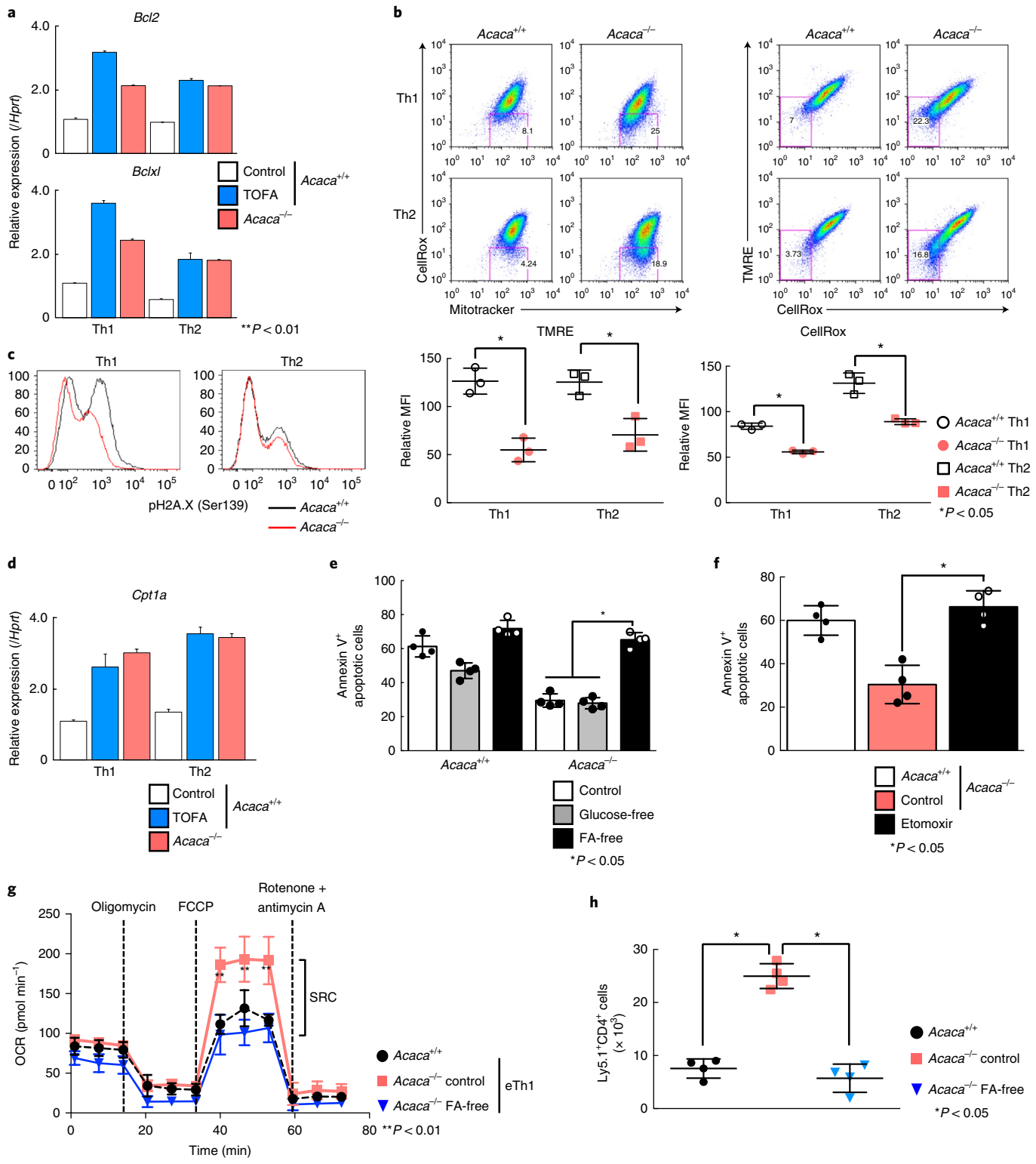

Supplementary Fig. 13c). For other differentially expressed surface molecules identified in Fig. 5 such as GPR34 and GIPR, no clear distinction was observed between *Acaca*$^{+/+}$ and *Acaca*$^{-/-}$ Th cells (Supplementary Fig. 13d).

These results prompted us to perform RNA-sequencing (RNA-seq) analysis to characterize the transcriptional profiles of these two populations (CCR7^{hi}CD137^{lo} and CCR7^{lo}CD137^{hi} populations) in early-differentiating effector cells in detail. A total of 157 genes showed greater than two-fold change (with a false discovery rate < 0.05), including 44 upregulated and 113 downregulated genes in the putative memory precursor CCR7^{hi}CD137^{lo} population (Fig. 6d, Supplementary Fig. 13e and Supplementary Table 1). Gene ontology and pathway analyses using the National Institute of Allergy and Infectious Diseases (NIAID) DAVID and KEGG databases showed significant enrichment of several functional categories, including cytokine receptor and activator in the upregulated genes, and apoptosis, repressor, and fatty acid biosynthesis in the downregulated genes (Fig. 6e). Gene expression analysis by

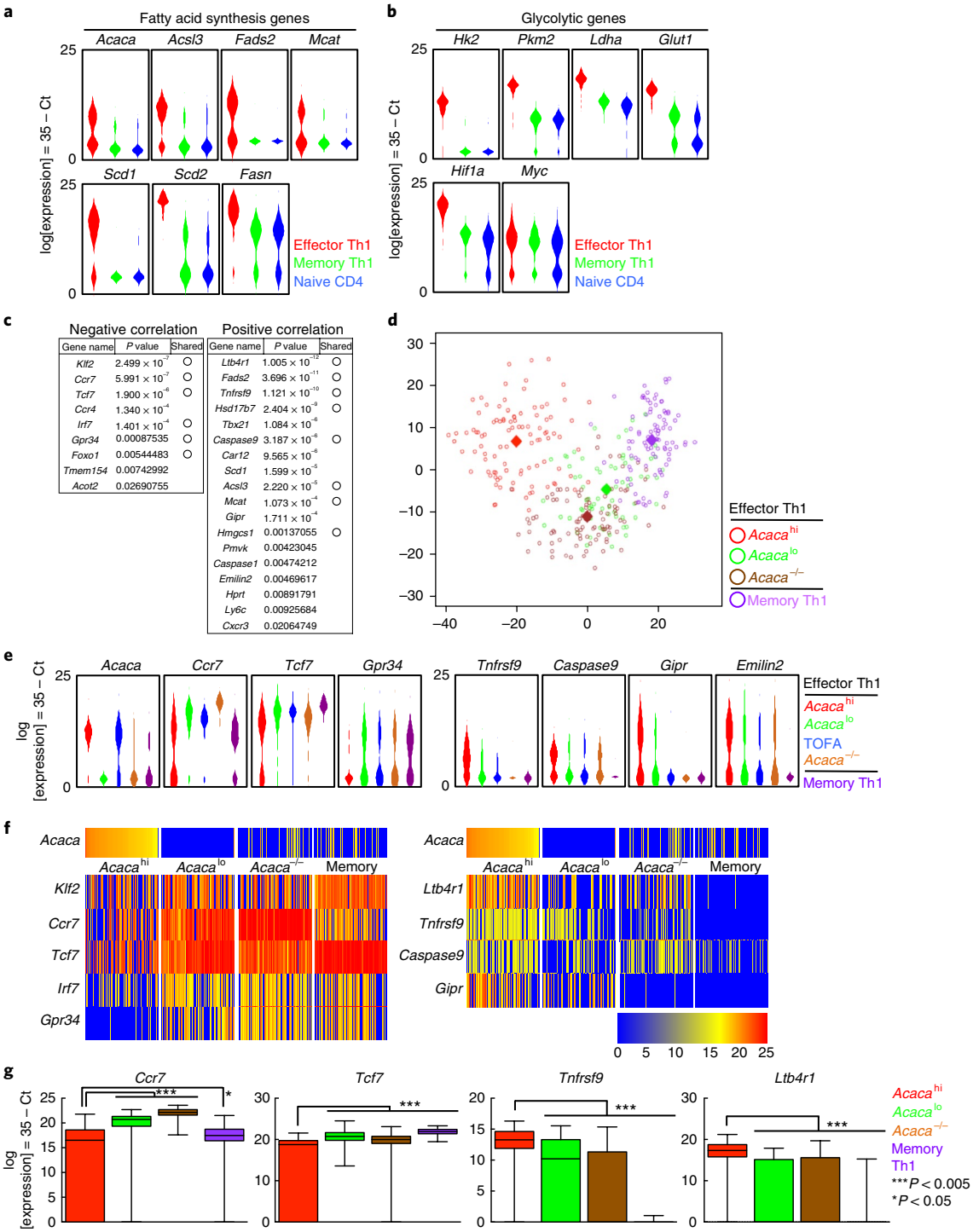

Fig. 5 | Acaca-correlated gene cluster allows prediction of cell fates of effector and memory CD4+ T cells. a,**b**, Expression of representative fatty acid synthesis genes (**a**) and representative glycolytic genes (**b**) in individual naive CD4+, effector Th1 and memory Th1 cells, presented as 'violin plots' (expression distribution defined as log of expression measured as 35 – Ct) ($n = 94$ single cell per group). **c**, Summary of chi-squared test results based on expression of *Acaca* at single-cell level. The top-ranked genes with *P* values shared between Th1 and Th2 cells are shown ($n = 94$ single cell per group). **d**, Projections of principal components 1 and 2 (PC1 and PC2) for *Acaca*-correlated genes derived from individual *Acaca*^{hi}-, *Acaca*^{lo}- and *Acaca*$^{-/-}$-effector and memory Th1 cells. PC1 and PC2 account for 25% and 10% of the variance, respectively. Color-coded diamonds represent median of each population (*Acaca*^{hi} PC1 = –20.2, PC2 = 6.8; *Acaca*^{lo} PC1 = 5.3, PC2 = –4.6; *Acaca*$^{-/-}$ PC1 = –0.2, PC2 = –11.0; and memory PC1 = 18.0, PC2 = 7.0) ($n = 67$ single cells for *Acaca*^{lo} group, and $n = 94$ single cells for other groups). **e**, Expression of representative *Acaca*-correlated genes in individual *Acaca*^{hi}-, *Acaca*^{lo}-, TOFA-treated- and *Acaca*$^{-/-}$-effector Th1 cells and memory Th1 cells, presented as violin plots ($n = 67$ single cells for *Acaca*^{lo} group, and $n = 94$ single cells for other groups). **f**, Heatmap visualization of *Acaca*-correlated genes in individual *Acaca*^{hi}-, *Acaca*^{lo}- and *Acaca*$^{-/-}$-effector and memory Th1 cells. Colors indicate expression of *Acaca*-correlated genes along left margin ($n = 94$ single cells per group). **g**, Quantification of results of heatmap plot of **f** ($n = 94$ single cells per group). Measure of center indicates mean ± s.d. ***$P < 0.005$, *$P < 0.05$ by two-tailed Mann-Whitney *U*-test. Three independent experiments were performed with similar results for **a**–**c**. Two independent experiments were performed with similar results for **d**–**g**.

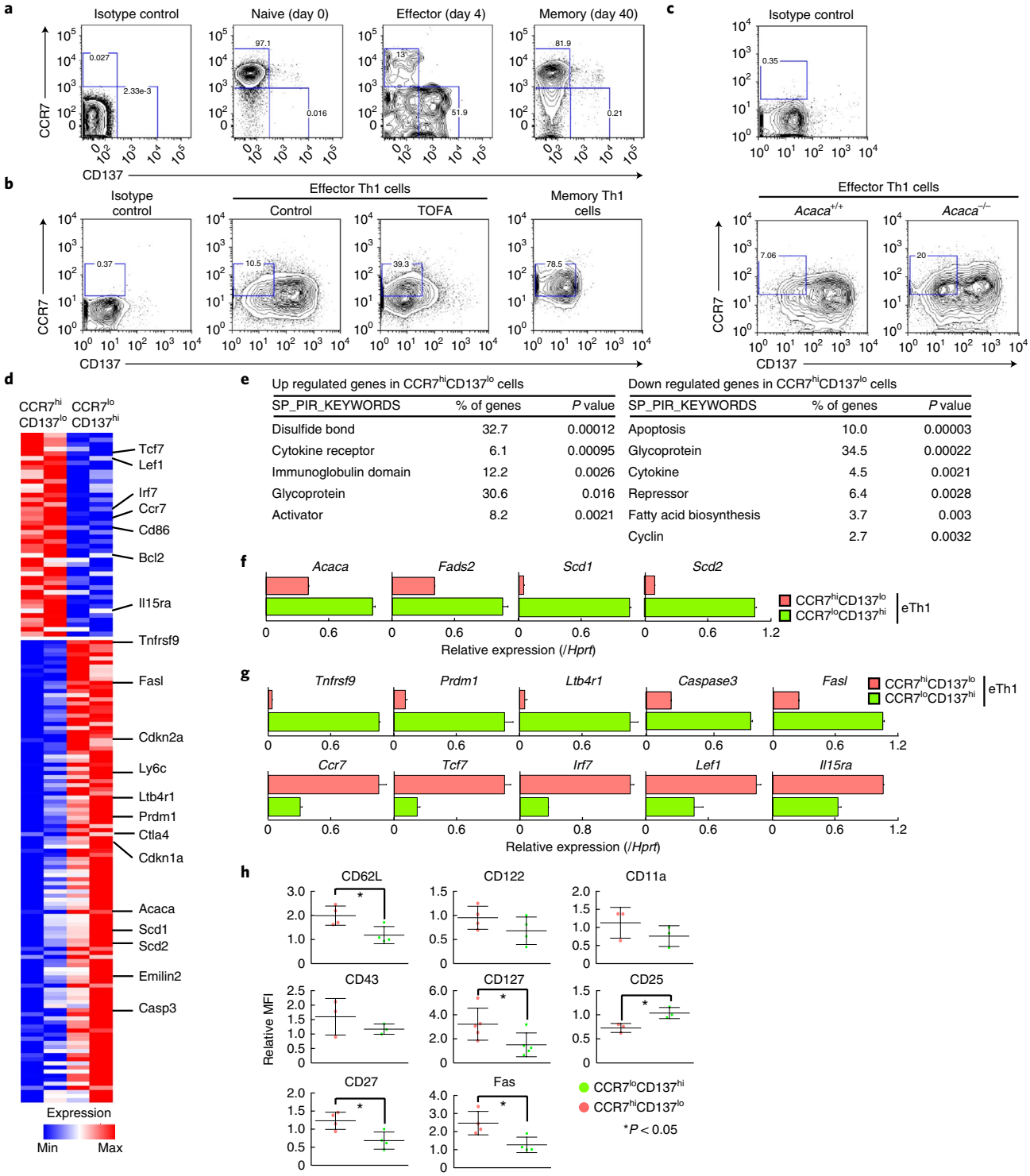

Fig. 6 | Segregation of CCR7 and CD137 expression during early effector cell differentiation influences transcriptional profiles. a, Cell surface expression profiles of CCR7 and CD137 on naive CD4$^+$ T cells, early-differentiating effector CD4$^+$ T cells (day 4 post-immunization) and memory CD4$^+$ T cells (day 40 post-immunization). **b**, Cell surface expression profiles of CCR7 and CD137 on TOFA-treated effector Th1 cells in vitro and memory Th1 cells. **c**, Cell surface expression profiles of CCR7 and CD137 on *Acaca*$^{+/+}$- or *Acaca*$^{-/-}$-effector Th1 cells. CCR7-positive or negative or CD137-positive or negative cells were determined by staining of these cells with isotype control antibody (**a**–**c**). **d**, Heatmap depicting differentially expressed genes in the CCR7^{hi}CD137^{lo} and the CCR7^{lo}CD137^{hi} populations of early-differentiating effector Th1 cells. **e**, RNA-seq analyses of CCR7^{hi}CD137^{lo} and CCR7^{lo}CD137^{hi} populations in early-differentiating effector Th1 cells ($n = 2$ biologically independent samples) were analyzed using DAVID and KEGG databases ($P < 0.01$, one-tailed EASE score, the modified Fisher's exact P value). The nature (keyword) of upregulated and downregulated genes are shown. **f**,**g**, Expression of fatty acid biosynthetic enzymes (**f**) and *Acaca*-correlated genes (**g**) in CCR7^{hi}CD137^{lo} (red) and CCR7^{lo}CD137^{hi} (green) Th1 cell populations. **h**, Summary data of relative MFI of cell surface staining in Supplementary Fig. 15 ($n = 3$ biologically independent samples). *$P < 0.05$ (one-way ANOVA with Mann-Whitney U-test (**h**)). Each symbol (**h**) represents an individual mouse; the measure of center (**f**–**h**) indicates mean ± s.d. Three technical replicates and four biological replicates were performed for quantitative rtPCR analysis (**f**,**g**). More than three independent experiments were performed with similar results for **a**–**c**,**f**–**h**.

quantitative rtPCR confirmed that expression of *Acaca*, *Fads2*, *Scd1* and *Scd2* was significantly lower in the CCR7^{hi}CD137^{lo} population than in the CCR7^{lo}CD137^{hi} population of early-differentiating effector Th1 cells (Fig. 6f), ovalbumin-specific early-differentiating effector CD4$^+$ T cells (Supplementary Fig. 13f) and human Th1 cells (Supplementary Fig. 14b). The expression of genes increased in early-differentiating effector cells, such as *Tnfrsf9*, *Prdm1*, *Ltb4r1*, *Casp3*, and *Fasl*, was lower in the CCR7^{hi}CD137^{lo} population than in the CCR7^{lo}CD137^{hi} population (Fig. 6g and Supplementary Fig. 13g). Notably, the expression of *Prdm1* (encoding Blimp1), reported to be critical for terminal differentiation of CD8 T cells but not memory formation[37,38], was significantly lower in the CCR7^{hi}CD137^{lo} population than in the CCR7^{lo}CD137^{hi} population (Fig. 6d,g and Supplementary Fig. 13g). In contrast, the expression of genes associated with the memory signature, including CCR7, *Tcf7*, *Irf7*, *Lef1* and *Il15ra*, was higher in the CCR7^{hi}CD137^{lo} population than in the CCR7^{lo}CD137^{hi} population. Similar results were detected in human effector Th1 cells (Supplementary Fig. 14c). These transcriptional analyses revealed that ACC1 may control not only Th17-regulatory T cell balance[26] but also the CD4$^+$ T cell effector-memory fate decision during early differentiation from naive into effector Th cells. Furthermore, we also characterized the expression of conventional effector and memory molecules in these two populations, and found that the expression of CD62L, CD127 (IL-7Rα), CD27 and Fas was significantly higher in the CCR7^{hi}CD137^{lo} population than in the CCR7^{lo}CD137^{hi} population of early-differentiating Th1 (Fig. 6h and Supplementary Fig. 15) and Th2 cells (Supplementary Fig. 13h). In contrast, the expression of CD25 (IL-2Rα) was lower in the CCR7^{hi}CD137^{lo} population than in the CCR7^{lo}CD137^{hi} population of early-differentiating Th1 (Fig. 6h and Supplementary Fig. 15) and Th2 cells[1,35,38] (Supplementary Fig. 13h). The expression of CD43 was comparable between the two, and KLRG1 was not detected in these populations (Fig. 6h). We further investigated whether supplementation of fatty acids to *Acaca*-deficient T cells could reverse the proportion of CCR7^{hi}CD137^{lo} cells in which memory precursors were highly enriched. Oleic acid strongly reversed the proportion of CCR7^{hi}CD137^{lo} population in *Acaca*-deficient cells, whereas supplementation with palmitic acid did not (Supplementary Fig. 13j).

We next compared the mitochondrial activity of the CCR7^{hi}CD137^{lo} and CCR7^{lo}CD137^{hi} populations. Oxygen consumption studies showed that the CCR7^{hi}CD137^{lo} population had significantly higher respiratory capacity, but the rate of glycolysis was not markedly different between the populations (Fig. 7a and Supplementary Fig. 13i). Furthermore, analysis of apoptosis revealed that the CCR7^{hi}CD137^{lo} population was comparatively resistant to cytokine withdrawal–induced apoptosis in both mice (Fig. 7b) and humans (Supplementary Fig. 14d).

Finally, we assessed the ability of these markers to identify cell populations with increased memory potential by transferring purified CCR7^{lo}CD137^{lo}, CCR7^{hi}CD137^{lo}, CCR7^{lo}CD137^{hi} and CCR7^{hi}CD137^{hi} early-differentiating Th1 cell populations into syngeneic recipient mice. The CCR7^{hi}CD137^{lo} population showed a robust and significant increase compared to CCR7^{lo}CD137^{lo} and CCR7^{lo}CD137^{hi} populations, and also a significant increase compared to the CCR7^{hi}CD137^{hi} population in efficiency of memory cell formation (Fig. 7c,d and Supplementary Fig. 16a,b). These results indicate that the combination of CCR7 and CD137 expression identifies the population in which memory precursors are highly enriched. We next rechallenged the mice that received CCR7^{hi}CD137^{lo} or CCR7^{lo}CD137^{hi} populations with ovalbumin intranasally, and monitored their expansion. The CCR7^{hi}CD137^{lo} population again persisted better and exhibited robust re-expansion after ovalbumin rechallenge (Fig. 7e,f, and Supplementary Fig. 16c).

Discussion

We show that after activation, most naive CD4$^+$ T cells differentiate into a ACC1^{hi}CCR7^{lo}CD137^{hi} effector cell population that is CD62L^{lo}IL-7Rα^{lo}IL-2Rα^{hi}CD27^{lo}Fas^{lo}Blimp1^{hi}TCF1^{lo} with a phenotype characterized by high fatty acid biosynthesis and low respiratory capacity. This population is relatively short lived, presumably owing to a failure to metabolically transition from activated to a quiescent state during the contraction phase (Fig. 7f). We also identified a smaller ACC1^{lo}CCR7^{hi}CD137^{lo} population that is CD62L^{hi}IL-7Rα^{hi} IL-2Rα^{lo} CD27^{hi}Fas^{hi}Blimp1^{lo}TCF1^{hi} with a phenotype characterized by low fatty acid biosynthesis and high respiratory capacity. This population is capable of long-term survival in vivo and can efficiently form memory cells. Although these populations may still have a great deal of heterogeneity, the memory Th cell precursor population is highly enriched in the CCR7^{hi}CD137^{lo} population of early-differentiating effector Th cells and has a unique transcriptional profile of memory signature genes.

In summary, we have identified a memory CD4$^+$ Th1 or Th2 cell precursor-enriched population (CCR7^{hi}CD137^{lo}) and demonstrated a critical link between ACC1-mediated fatty acid metabolism and memory T-cell fate determination. Our findings have implications for understanding memory cell fate determination in antigen-stimulated effector CD4$^+$ T cells via mechanistic insights into cellular metabolism. In addition, the identification of markers of memory precursors may prove valuable for vaccine development and adoptive immunotherapy approaches.

Fig. 7 | Segregation of CCR7 and CD137 expression during early effector cell differentiation influences metabolic signature and cell fates. a, OCR of CCR7^{hi}CD137^{lo} and CCR7^{lo}CD137^{hi} Th1 cell populations ($n=4$ biologically independent samples per group). **b**, Susceptibility to apoptosis of CCR7^{hi}CD137^{lo} and CCR7^{lo}CD137^{hi} Th1 cell populations was investigated by annexin V and PI. Summary data of apoptosis assay were also shown ($n=4$ biologically independent samples per group). **c**,**d**, Summary data for memory Th1 cells (Thy1.1$^+$) in CD4$^+$ splenocytes from mice receiving CCR7^{lo}CD137^{lo} (grey), CCR7^{hi}CD137^{lo} (red), CCR7^{lo}CD137^{hi} (green) or CCR7^{hi}CD137^{hi} (blue) Th1 cell populations ($n=6$ biologically independent samples per each group). **e**, Ovalbumin-specific early-differentiating effector CD4$^+$ T cells (day 4 post-immunization) were subjected to cell sorting for CCR7^{hi}CD137^{lo} and CCR7^{lo}CD137^{hi} populations, and these cells (1×10^6 cells per mouse) were transferred separately into syngeneic BALB/c mice. On day 40, the mice were challenged intranasally with ovalbumin. The proportion or cell number of donor-derived KJ1.26$^+$ memory CD4$^+$ T cells in the lung was determined by flow cytometry (CCR7^{hi}CD137^{lo}, red, $n=5$; CCR7^{lo}CD137^{hi}, green, $n=5$ biologically independent samples). **f**, Most naive CD4$^+$ T cells differentiate into a CCR7^{lo}CD137^{hi} CD62L^{lo}IL-7Rα^{lo}IL-2Rα^{hi}CD27^{lo}Fas^{lo}IL-15Rα^{lo}LTB4R1^{hi}FASL^{hi}Blimp1^{hi}TCF1^{lo} Th1 or Th2 cell population with higher expression of *Acaca*, *Fads2*, *Scd1* and *Scd2* that is characterized by high fatty acid biosynthesis and low respiratory capacity. This population is relatively short lived presumably owing to the failure of metabolic transition from metabolically activated to quiescent status during the contraction phase. A minor CCR7^{hi}CD137^{lo}CD62L^{hi}IL-7Rα^{hi} IL-2Rα^{lo}CD27^{hi}Fas^{hi}IL-15Rα^{hi}LTB4R1^{lo}FASL^{lo}Blimp1^{lo}TCF1^{hi} cell population shows low fatty acid biosynthesis and high respiratory capacity. This population has lower expression of *Acaca*, *Fads2*, *Scd1* and *Scd2*, and shows long-term survival and efficient memory cell generation, and thus the memory Th cell precursor population is enriched in the CCR7^{hi}CD137^{lo} population with unique transcriptional profiles of memory signature genes, higher levels of *Tcf7*, *Irf7*, *Lef1* and lower levels of *Prdm1* and *Caspase3*. $^{**}P<0.01$, $^{*}P<0.05$ (two-tailed Student's *t*-test (**a**–**e**)). Each symbol (**b**–**e**) represents an individual mouse; the measure of center (**a**–**f**) indicates mean ± s.e.m (**c**–**d**) or s.d (**a**,**b**)). Four biological replicates were performed for seahorse analysis (**a**). Two independent experiments were performed with similar results for **a**–**e**.

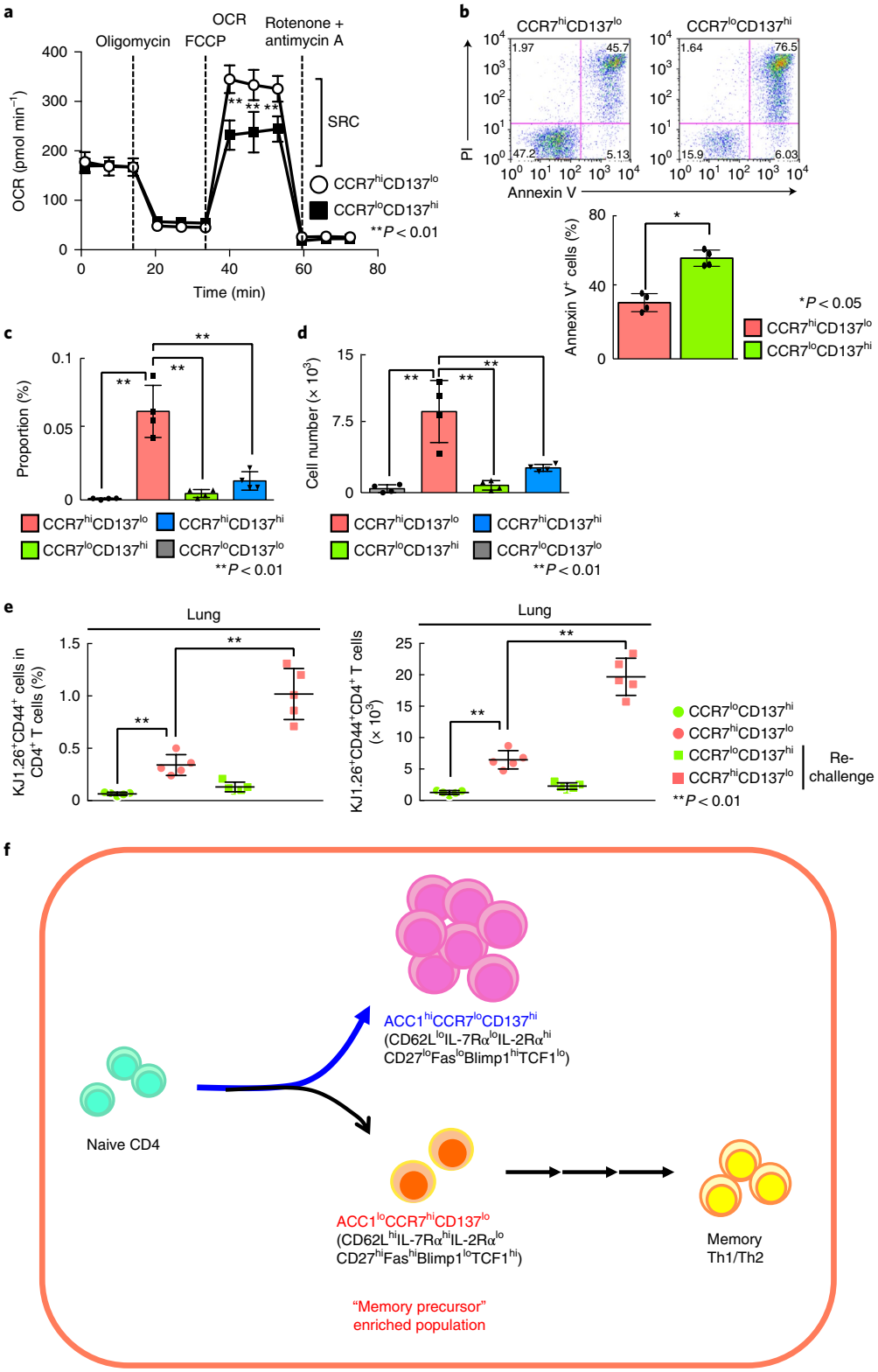

Methods

Mice. The animals used in this study were backcrossed to BALB/c or C57BL/6 mice ten times. *Acaca*$^{fl/fl}$ mice[30] were crossed with CD4-cre or ERT2-cre mice (Jackson Laboratory) and were maintained on a C57BL/6 background. Ovalbumin-specific TCR-αβ (DO11.10) transgenic mice were provided by D. Loh (Washington University School of Medicine)[39]. Ly5.1 and Thy1.1 mice were purchased from Sankyo Laboratory. C57BL/6 mice and BALB/c mice were purchased from Clea. All of the mice were used at 6–8 weeks of age and maintained under specific-pathogen-free conditions. For all experiments, age-matched (7–14 weeks) and sex-matched littermate mice maintained under specific-pathogen-free conditions were used. The research proposals were reviewed by the ethics committee for animals at Chiba University (registration number 29-98, 29-99).

Reagents. The reagents used in this study were as follows: FITC-, APC-, PE/Cy7-, BV421- and BV510-conjugated anti-CD4 (FITC, 100406; PE, 100408; APC, 100412; PE/Cy7, 100422; BV421, 100438; BV510, 100449; GK1.5, 1 μg ml^{-1}); PE-conjugated anti-CD8 (100708, 53-6.7, 1 μg ml^{-1}), PE-, APC- and PE/Cy7-conjugated anti-CD62L (PE, 104408; APC, 104412; PE/Cy7, 104418; MEL-14, 1 μg ml^{-1}); FITC- and PE-conjugated anti-CD44 (FITC, 103006; PE, 103024; IM7,

1 μg ml^{-1}); FITC- and BV-421-conjugated Ly5.2 (FITC, 109806; BV421, 109382; 104, 1 μg ml^{-1}) and Ly5.1 (FITC, 110706; BV421, 110732; A20, 1 μg ml^{-1}); PE/Cy7-conjugated Thy1.2 (105326, 30-H12, 1 μg ml^{-1}) and Thy1.1 (202518, OX-7, 1 μg ml^{-1}); PE-conjugated anti-CCR7 (120106, 4B12, 1 μg ml^{-1}), anti-GL7 (144608, GL7, 1 μg ml^{-1}) and anti-PD1 (135206, 29F.1A12, 1 μg ml^{-1}); APC-conjugated anti-CD137 (106110, 17B5, 1 μg ml^{-1}) and anti-KLRG1 (138412, 2F1/KLRG1, 1 μg ml^{-1}); Alexa647-conjugated anti-Foxp3 (126408, MF-14, 1 μg ml^{-1}); FITC-conjugated anti-CD11a (101106, M17/4, 1 μg ml^{-1}), anti-CD25 (101908, 3C7, 1 μg ml^{-1}), anti-CD27 (124208, LG.3A10, 1 μg ml^{-1}), anti-CD43 (121206, 1B11, 1 μg ml^{-1}), anti-122 (123208, TM-β1, 1 μg ml^{-1}), anti-CD127 (135008, A7R34, 1 μg ml^{-1}), anti-KJ1 (118506, KJ1-26, 1 μg ml^{-1}) and anti-Fas (152606, SA367H8, 1 μg ml^{-1}) and APC/cy7-conjugated anti-CXCR5 (145526, L138D7, 1 μg ml^{-1}) were purchased from BioLegend. Alexa 488-conjugated anti-GPR34, anti-GIPR and anti-TCF1 (6444, C63D9, 1 μg ml^{-1}) and Alexa 647-conjugated anti-pH2A.X (Ser139) (9720, 20E3, 1 μg ml^{-1}) were purchased from Cell Signaling. TOFA, 3-bromopyruvate, rapamycin and etomoxir purchased from Merck were used as pharmacological inhibitors. CellRox, Mitotracker and TMRE were purchased from Thermo Fisher Scientific.

Mouse T cell cultures. Naive (CD44^{lo}CD62L^{hi}) CD4 T cells were purified from the spleens of mice. After lysis of red blood cells, the CD4$^+$ T cells were obtained using a CD4 T cell isolation kit with anti-CD4 microbeads (Miltenyi Biotec), and naive CD44^{lo}CD62L^{hi} cells were then further sorted to >99.5% purity using a fluorescence-activated cell sorting (FACS) Aria cell sorter (BD Biosciences). Naive CD4$^+$ T cells were plated onto 24-well tissue culture plates (Costar) precoated with 10 μg ml^{-1} agonistic antibody to TCR-λ (clone H57-597) with 1 μg ml^{-1} agonistic antibody to CD28 (clone 37.51; Biolegend). The Th1 cell cultures contained IL-2 (15 ng ml^{-1}), recombinant mouse IL-12 (10 ng ml^{-1}) (Wako) and antibody to IL-4 (BD Bioscience, BVD4-1D11). The Th2 cell cultures contained IL-2 (15 ng ml^{-1}), recombinant mouse IL-4 (100 ng ml^{-1}) (Peprotech) and antibody to IFN-γ (Biolegend, R4-6A2). The Th17 cell cultures contained antibody to IL-2 (BD biosciences), recombinant mouse IL-6 (Peprotech) (10 ng ml^{-1}), recombinant human TGF-β (1 ng ml^{-1}) (Peprotech), recombinant mouse IL-1β (10 ng ml^{-1}) (Peprotech), recombinant mouse IL-23 (10 ng ml^{-1}) (R&D Systems) and antibodies to IL-4 and IFN-γ. Oleic acid or palmitic acid (Sigma-Aldrich) was dissolved in ethanol with a final concentration of 100 mM or 10 mM, respectively, and was complexed to BSA. *Acaca*$^{fl/fl}$ naive CD4 T cells were cultured under Th1 conditions in the presence of the indicated concentrations of fatty acids.

Human T cell cultures. Whole blood was obtained from healthy donor volunteers with given consent. The research proposals were reviewed by the ethics committee at Chiba University (registration number 1016). Human CD4$^+$ T cells were collected by a Ficoll gradient. For human naive CD4$^+$ T cells, CD45RA$^+$CD45RO$^-$ cells were collected using a FACS Aria cell sorter (BD Biosciences). Human naive CD4$^+$ T cells were plated onto 48-well tissue culture plates (Costar) precoated with 1 μg ml^{-1} anti-CD3 (clone OKT3) with 1 μg ml^{-1} anti-CD28 (clone CD28.2) in the presence or absence of TOFA. Th1 cell cultures contained IL-2 (15 ng ml^{-1}), IL-12 (15 ng ml^{-1}) and antibody to IL-4 (1 μg ml^{-1}), and Th2 cell cultures contained IL-2 (15 ng ml^{-1}), IL-4 (15 ng ml^{-1}), and antibody to IFN-γ (1 μg ml^{-1}).

Generation of effector and memory Th1 and Th2 cells. Effector and memory Th1 and Th2 cells were generated as described[40]. Splenic CD62L$^+$CD44$^-$ naive KJ1$^+$CD4$^+$ T cells from DO11.10 ovalbumin-specific TCR transgenic mice, or ERT2-cre$^+$*Acaca*$^{+/+}$ or ERT2-cre$^+$*Acaca*$^{fl/fl}$ (*Acaca*$^{-/-}$) naive CD4$^+$ T cells from OTII transgenic mice, were stimulated with an ovalbumin peptide (Loh15, 1 μM) plus APC (irradiated splenocytes) under Th1- or Th2-culture conditions for 6 d in vitro. 4-OHT (100 nM) was added into cultures on day 2. In some experiments, differentiating Th cells were treated with TOFA (10 μM), rapamycin (5 nM) or 3-bromopyruvate (10 μM) on day 2. These effector Th1 or Th2 cells (1×10^7) were transferred intravenously into BALB/c *nu/nu*, BALB/c recipient mice or syngeneic C57BL/6 mice. At 5 weeks after the cell transfer, KJ1$^+$CD4$^+$ T cells or Ly5.1$^+$ cells in organs including spleen, lymph nodes, lung and liver were analyzed. For the detection of cytokine production, KJ1$^+$CD4$^+$ T cells or Ly5.1$^+$ donor cells in the spleen were purified by auto-MACS (Miltenyi Biotec) and cell sorting (BD Aria II) and then were stimulated with phorbol myristate acetate (PMA) plus ionomycin. In some experiments, *Acaca*$^{+/+}$ or *Acaca*$^{-/-}$ effector Th1 cells were cultured under glucose-free (RPMI 1640 medium, no glucose; 11879020, Sigma) or fatty acid–free (BSA, fatty acid–free; 011-15144, Wako) conditions.

Generation of antigen-specific effector and memory CD4$^+$ T cells. Splenic CD62L$^+$CD44$^-$ naive KJ1$^+$CD4$^+$ T cells from Thy1.1$^+$DO11.10 ovalbumin-specific TCR transgenic mice were transferred intravenously into BALB/c recipient mice. These mice were injected with alum (Thermo Fisher Scientific)–emulsified ovalbumin on day 1. Ovalbumin-immunized BALB/c mice were treated with TOFA (from day −1 to day 4 post-immunization) or not treated. Ovalbumin-specific effector CD4$^+$ T cells were analyzed on day 5, and memory CD4$^+$ T cells were analyzed on day 40. Recall responses were analyzed on day 42 after ovalbumin rechallenge. For detection of ovalbumin-responsive memory CD4$^+$ T cells, Vα2$^+$CD44^{hi}Foxp3$^-$CD4$^+$ T cells were measured. For analysis of kinetics of ovalbumin-specific KJ1$^+$CD4$^+$ T cells, peripheral blood mononuclear cell (PBMCs) of ovalbumin-immunized BALB/c mice were analyzed using FACS. For CCR7/CD137 subpopulation experiments, each subpopulation was separated based on the expression of CCR7 and CD137 on day 2 or 3, and subsequently these populations were analyzed with RNA-seq or seahorse assay, or injected into other syngeneic BALB/c mice.

Conditional deletion of *Acaca* on memory CD4$^+$ T cells. Splenic ERT2-cre$^+$*Acaca*$^{+/+}$ or ERT2-cre$^+$*Acaca*$^{fl/fl}$ naive CD4$^+$ T cells from Ly5.1$^+$OTII transgenic mice were transferred intravenously into syngeneic C57BL/6 recipient mice. These mice were injected with alum-emulsified ovalbumin on day 1. Subsequently, mice were injected (i.p.) with 3.125 μl of tamoxifen dissolved in corn oil at a concentration of 10 mg ml^{-1} from days 2 to 6. Ovalbumin-specific memory CD4$^+$ T cells were analyzed on day 40. Recall responses were analyzed on day 42 after ovalbumin rechallenge. In some experiments, *Acaca*$^{+/+}$ or CD4-cre$^+$*Acaca*$^{fl/fl}$ mice were directly injected with alum-emulsified ovalbumin on day 1. Ovalbumin-specific memory CD4$^+$ T cells were analyzed on day 40. Recall responses were analyzed on day 4 after ovalbumin rechallenge. For analysis of kinetics of ovalbumin-specific KJ1$^+$CD4$^+$ T cells, PBMCs of ovalbumin-immunized BALB/c mice were analyzed using FACS.

Helminth infection. Splenic ERT2-cre$^+$*Acaca*$^{+/+}$ or ERT2-cre$^+$*Acaca*$^{fl/fl}$ naive CD4$^+$ T cells from Ly5.1$^+$ or Ly5.1$^+$5.2$^+$ mice were transferred intravenously into syngeneic C57BL/6 recipient mice. These mice were infected with Nb by subcutaneous injection of 500 third-stage larvae (L3). Subsequently, mice were injected (i.p.) with 3.125 μl of tamoxifen dissolved in corn oil at 10 mg ml^{-1} from days 10 to 14. Memory CD4$^+$ T cells were analyzed on day 40. Recall responses were analyzed on day 45 after helminth re-infection. In some experiments, *Acaca*$^{+/+}$ or CD4-cre$^+$*Acaca*$^{fl/fl}$ mice were directly infected with Nb by subcutaneous injection of 500 third-stage larvae (L3) on day 1. Subsequently, these mice were re-infected with 2,000 Nb L3 on day 40. The absolute number of worms in the small intestine on day 7 after subcutaneous inoculation of Nb L3 was analyzed. For follicular helper T cells and germinal center detection, CXCR5$^+$PD-1$^+$ expression on donor-derived Ly5.1$^+$CD4$^+$ T cells for follicular helper T cells or Fas$^+$GL7$^+$ expression on B220$^+$ cells for germinal center cells in the spleen was analyzed.

Enzyme-linked immunosorbent assay for antibodies. NP-specific antibodies in serum were measured by plate-coated NP_4- and NP_{48}-BSA. Hapten-specific antibodies were detected with alkaline phosphatase–conjugated antibodies to mouse IgG1 (Southern Biotechnology).

Detection of apoptotic cells. For detection of apoptotic cells, an Annexin V^{FITC} apoptosis detection kit II (BD Biosciences) was used in accordance with the manufacturer's protocol.

Gene chip hybridization of microarrays and data analysis. DNA microarray analysis of gene expression was performed at Takara Bio. A 250-ng aliquot of total RNA from each sample was hybridized to a GeneChip Mouse Genome 430.2.0 array (Affymetrix). The expression values were determined with the GeneChip Operating Software (GCOS) program. A more than two-fold increase or decrease in the sample groups as compared to other sample groups was defined as significant (with a false discovery rate < 0.05). Gene ontology analysis was performed using the NIAID DAVID website (http://david.abcc.ncifcrf.gov) with statistical analysis (*P* values).

Metabolic profiling. Unbiased metabolic profiling was performed by Human Metabolome Technologies using ovalbumin-specific control, TOFA-treated, rapamycin treated and *Acaca*$^{-/-}$ effector Th1 cells and memory Th1 cells. At the end of culturing, 50 million cells were spun down and the pellets were washed with 5% mannitol before being frozen in methanol with internal standard solution (10 μM). Relative quantities of each metabolite were estimated by comparison of peak area with that of a standard compound in Internal Standard Solution 1, and the values were determined as relative peak area. In data processing of relative peak area, the metabolites detected in triplicate were used for calculation of means, standard deviations and other analyses. All the samples were analyzed through capillary electrophoresis time-of-flight mass spectrometry at Human Metabolome Technologies.

Seahorse analysis. The OCR and extracellular acidification rate were measured with an XF96 analyzer (Seahorse Bioscience). In detail, cultured CD4 T cells were seeded at a density of 200,000 cells per well on a XF96 cell culture microplate. Before assay, cells were equilibrated for 1 h in unbuffered XF assay medium supplemented with 25 mM glucose and 1 mM sodium pyruvate. Mixing, waiting and measure times were 2, 2 and 4 min, respectively. Compounds were injected during the assay at the following final concentrations: 0.2 μM oligomycin, 0.5 μM FCCP and 0.75 μM rotenone-antimycin A.

Quantitative real-time PCR. Total RNA was isolated using the TRIzol reagent (Invitrogen). cDNA was synthesized using oligo(dT) primers and Superscript II RT

(Invitrogen). Quantitative rtPCR was performed as described previously[25] using an ABI PRISM 7500 Sequence Detection System. The primers and TaqMan probes were purchased from Applied Biosystems. The primers and Roche Universal probes used were purchased from Sigma and Roche, respectively. Gene expression was normalized using the *Hprt* mRNA signal or the *18S* ribosomal RNA signal.

RNA sequencing. Total cellular RNA was extracted with TRIzol reagent (Invitrogen). For cDNA library construction, we used TruSeq RNA Sample Prep Kit v2 (Illumina) according to the manufacturer's protocol. Sequencing the library fragments was performed on the HiSeq 2500 system. For data analysis, read sequences (50 bp) were aligned to the mm10 mouse reference genome (University of California Santa Cruz, December 2011) using Bowtie (version 0.12.8) and TopHat (version 1.3.2). Fragments per kilobase of exon per million mapped reads (FPKM) for each gene were calculated using Cufflinks (version 2.0.2). Genes with an absolute FPKM > 1 (mean from duplicate samples) were defined as expressed genes.

Single-cell quantitative rtPCR. The primer pairs were pooled together in DNA Suspension buffer (Teknova) to a final concentration of 0.2× for each of the 96 gene-expression assays. Single $CD4^+$ T cells were sorted directly into RT-PreAmp Master Mix (Life Technologies) containing the pooled assays using an Aria cell sorter. Cell lysis, sequence-specific reverse transcription and sequence-specific amplification of cDNA were performed in accordance with the manufacturer's protocol. High-throughput quantitative PCR was done on 96.96 Dynamic Arrays with a BioMark system (Fluidigm). The cycling threshold values were calculated with the BioMark system software program from SINGuLar. After completion of the initial quantitative PCR analysis using BioMark Realtime PCR analysis software, data were exported using the 'export heatmap' option, which generates comma-separated value (*.csv) files suitable for import into R using script packages produced by Fluidigm—SINGuLar Analysis Toolsets 2.1 and 3.0.

Data and processing. The log expression of each gene was computed as follows: log[expression] = 35 – Ct, where Ct is the cycling threshold value obtained from the BioMark (Fluidigm). Cells with undefined cycling threshold values (Ct = 999) for both gene *Gapdh* and gene *Actb* were also removed from our analyses. The remaining cells in each population were deemed sufficient for all subsequent analysis. Data sets with outliers removed were used for further analysis using the autoAnalysis command in SINGuLar. Briefly, this command performs a series of statistical analyses on the data sets and additional commands can be used to further evaluate the data sets. We used PCA to diminish dimensionality of the data with a linear transformation and projected data from their original 96 dimensions to the first two principal components. The data were then plotted in two dimensions, with the first two principal components on opposing axes, and with each point on the PCA scatter plot representing an individual single-cell sample with relative positions reflecting similarity on the basis of the first two principal components. Based on the log[expression] = 35 – Ct of *Acaca* and other 95 genes at the single-cell level, the genes negatively correlated with or positively correlated with *Acaca* were obtained by chi-squared test.

Statistical analysis and general methods. Data are expressed as mean ± s.d. or mean ± s.e.m. The data were analyzed with the Graphpad Prism software program (version 6). Differences were assessed using two-tailed Student's *t*-tests, or nonparametric Mann-Whitney *U*-test where appropriate. Differences with $P < 0.05$ or 0.01 were considered to be significant. Sample size for animal studies was chosen based on prior experience with similar models of memory cell formation. No data were excluded from the analysis of experiments. Mice were commercially sourced and randomized into experimental groups upon arrival, and all animals within a single experiment were processed at the same time. For cell sorting and RNA-seq analysis the investigator was blinded. For cell transfer experiments the investigator was not blinded. Data display similar variance between groups and are normally distributed where parametric tests are used.

Reporting Summary. Further information on research design is available in the Nature Research Reporting Summary linked to this article.

Data availability

All data presented in this article are available in the main and supplementary figures, or upon request from corresponding authors. RNA-seq, microarray and single-cell rtPCR data in this manuscript are available in the Gene Expression Omnibus database (http://www.ncbi.nlm.nih.gov/geo) under accession number GSE122863 (SuperSeries). All data that support the findings of this study are available from the corresponding author upon reasonable request.

Received: 18 May 2018; Accepted: 7 December 2018;
Published online: 14 January 2019

References

1. Chang, J. T., Wherry, E. J. & Goldrath, A. W. Molecular regulation of effector and memory T cell differentiation. *Nat. Immunol.* **15**, 1104–1115 (2014).
2. Pulendran, B. & Ahmed, R. Immunological mechanisms of vaccination. *Nat. Immunol.* **12**, 509–517 (2011).
3. Sallusto, F., Lanzavecchia, A., Araki, K. & Ahmed, R. From vaccines to memory and back. *Immunity* **33**, 451–463 (2010).
4. Maus, M. V. et al. Adoptive immunotherapy for cancer or viruses. *Annu. Rev. Immunol.* **32**, 189–225 (2014).
5. Vanneman, M. & Dranoff, G. Combining immunotherapy and targeted therapies in cancer treatment. *Nat. Rev. Cancer* **12**, 237–251 (2012).
6. Nakayama, T. et al. Th2 cells in health and disease. *Annu. Rev. Immunol.* **35**, 53–84 (2017).
7. Williams, M. A. & Bevan, M. J. Effector and memory CTL differentiation. *Annu. Rev. Immunol.* **25**, 171–192 (2007).
8. Endo, Y., Hirahara, K., Yagi, R., Tumes, D. J. & Nakayama, T. Pathogenic memory type Th2 cells in allergic inflammation. *Trends Immunol.* **35**, 69–78 (2014).
9. Stockinger, B., Bourgeois, C. & Kassiotis, G. CD4+ memory T cells: functional differentiation and homeostasis. *Immunol. Rev.* **211**, 39–48 (2006).
10. Jameson, S. C. & Masopust, D. Diversity in T cell memory: an embarrassment of riches. *Immunity* **31**, 859–871 (2009).
11. Pearce, E. L. et al. Enhancing CD8 T-cell memory by modulating fatty acid metabolism. *Nature* **460**, 103–107 (2009).
12. O'Sullivan, D. et al. Memory CD8(+) T cells use cell-intrinsic lipolysis to support the metabolic programming necessary for development. *Immunity* **41**, 75–88 (2014).
13. Wang, R. & Green, D. R. Metabolic checkpoints in activated T cells. *Nat. Immunol.* **13**, 907–915 (2012).
14. MacIver, N. J., Michalek, R. D. & Rathmell, J. C. Metabolic regulation of T lymphocytes. *Annu. Rev. Immunol.* **31**, 259–283 (2013).
15. Pearce, E. L. & Pearce, E. J. Metabolic pathways in immune cell activation and quiescence. *Immunity* **38**, 633–643 (2013).
16. Cui, G. et al. IL-7-induced glycerol transport and tag synthesis promotes memory CD8+ T cell longevity. *Cell* **161**, 750–761 (2015).
17. Zeng, H. et al. mTORC1 couples immune signals and metabolic programming to establish T(reg)-cell function. *Nature* **499**, 485–490 (2013).
18. Okoye, I. et al. T cell metabolism. The protein LEM promotes CD8(+) T cell immunity through effects on mitochondrial respiration. *Science* **348**, 995–1001 (2015).
19. Araki, K. et al. mTOR regulates memory CD8 T-cell differentiation. *Nature* **460**, 108–112 (2009).
20. Bantug, G. R., Galluzzi, L., Kroemer, G. & Hess, C. The spectrum of T cell metabolism in health and disease. *Nat. Rev. Immunol.* **18**, 19–34 (2018).
21. Sukumar, M. et al. Inhibiting glycolytic metabolism enhances CD8+T cell memory and antitumor function. *J. Clin. Invest.* **123**, 4479–4488 (2013).
22. Kidani, Y. et al. Sterol regulatory element-binding proteins are essential for the metabolic programming of effector T cells and adaptive immunity. *Nat. Immunol.* **14**, 489–499 (2013).
23. Angela, M. et al. Fatty acid metabolic reprogramming via mTOR-mediated inductions of PPARgamma directs early activation of T cells. *Nat. Commun.* **7**, 13683 (2016).
24. Pan, Y. et al. Survival of tissue-resident memory T cells requires exogenous lipid uptake and metabolism. *Nature* **543**, 252–256 (2017).
25. Endo, Y. et al. Obesity drives th17 cell differentiation by inducing the lipid metabolic kinase, ACC1. *Cell Rep.* **12**, 1042–1055 (2015).
26. Berod, L. et al. De novo fatty acid synthesis controls the fate between regulatory T and T helper 17 cells. *Nat. Med.* **20**, 1327–1333 (2014).
27. Endo, Y., Yokote, K. & Nakayama, T. The obesity-related pathology and Th17 cells. *Cell. Mol. Life Sci.* **74**, 1231–1245 (2017).
28. Best, J. A. et al. Transcriptional insights into the CD8(+) T cell response to infection and memory T cell formation. *Nat. Immunol.* **14**, 404–412 (2013).
29. Lee, J. et al. Regulator of fatty acid metabolism, acetyl coenzyme a carboxylase 1, controls T cell immunity. *J. Immunol.* **192**, 3190–3199 (2014).
30. Mao, J. et al. Liver-specific deletion of acetyl-CoA carboxylase 1 reduces hepatic triglyceride accumulation without affecting glucose homeostasis. *Proc. Natl Acad. Sci. USA* **103**, 8552–8557 (2006).
31. Barnden, M. J., Allison, J., Heath, W. R. & Carbone, F. R. Defective TCR expression in transgenic mice constructed using cDNA-based alpha- and beta-chain genes under the control of heterologous regulatory elements. *Immunol. Cell Biol.* **76**, 34–40 (1998).
32. Fulda, S., Galluzzi, L. & Kroemer, G. Targeting mitochondria for cancer therapy. *Nat. Rev. Drug. Discov.* **9**, 447–464 (2010).
33. Sukumar, M. et al. Mitochondrial membrane potential identifies cells with enhanced stemness for cellular therapy. *Cell. Metab.* **23**, 63–76 (2016).
34. van der Windt, G. J. et al. Mitochondrial respiratory capacity is a critical regulator of CD8+ T cell memory development. *Immunity* **36**, 68–78 (2012).
35. Arsenio, J. et al. Early specification of CD8+T lymphocyte fates during adaptive immunity revealed by single-cell gene-expression analyses. *Nat. Immunol.* **15**, 365–372 (2014).
36. Ishizuka, I. E. et al. Single-cell analysis defines the divergence between the innate lymphoid cell lineage and lymphoid tissue-inducer cell lineage. *Nat. Immunol.* **17**, 269–276 (2016).

37. Rutishauser, R. L. et al. Transcriptional repressor Blimp-1 promotes CD8(+) T cell terminal differentiation and represses the acquisition of central memory T cell properties. *Immunity* **31**, 296–308 (2009).
38. Xin, A. et al. A molecular threshold for effector CD8(+ T cell differentiation controlled by transcription factors Blimp-1 and T-bet. *Nat. Immunol.* **17**, 422–432 (2016).
39. Murphy, K. M., Heimberger, A. B. & Loh, D. Y. Induction by antigen of intrathymic apoptosis of CD4+CD8+TCRlo thymocytes in vivo. *Science* **250**, 1720–1723 (1990).
40. Endo, Y. et al. The interleukin-33-p38 kinase axis confers memory T helper 2 cell pathogenicity in the airway. *Immunity* **42**, 294–308 (2015).

Acknowledgements

We thank S.J. Wakil (Baylor College of Medicine) for providing the *Acaca*$^{fl/fl}$ mice and M. Papadopoulos for critical reading and providing valuable suggestions on the manuscript. We also thank K. Sugaya and M. Kato for their excellent technical assistance. This work was supported by the Global COE Program (Global Center for Education and Research in Immune System Regulation and Treatment) and by grants from the Ministry of Education, Culture, Sports, Science and Technology (MEXT Japan) (grants-in-aid for Scientific Research [S] 26221305, [B] 21390147, and [C] 15K08522, Young Scientists [A] 16H06224, [B] 24790461, and 26870172, Challenging Research (Pioneering) 18H05375, grant-in-aid for Scientific Research on Innovative Areas (research in a proposed research area) 16H01352, 18H04665), AMED-CREST, AMED (P18gm1210003, JP16gm0410009), Practical Research Project for Allergic Diseases and Immunology from AMED (JP17ek0410030), the Ministry of Health, Labor and Welfare, the Astellas Foundation for Research on Metabolic Disorders, Ono Medical Research Foundation, Kanae Foundation for the Promotion of Medical Science, and Takeda Science Foundation.

Author contributions

Y.E., A.O., D.J.T., H.K. and T.N. designed experiments, analyzed the data and wrote the manuscript. Y.E., K.O.N., R.N., H.K.A., T.I., T.N., T.K., K.I. and TY performed experiments.

Competing interests

The authors declare no competing interests.

Additional information

Supplementary information is available for this paper at https://doi.org/10.1038/s42255-018-0025-4.

Reprints and permissions information is available at www.nature.com/reprints.

Correspondence and requests for materials should be addressed to T.N.

Publisher's note: Springer Nature remains neutral with regard to jurisdictional claims in published maps and institutional affiliations.

nature research

Corresponding author(s): Toshinori Nakayama

Reporting Summary

Nature Research wishes to improve the reproducibility of the work that we publish. This form provides structure for consistency and transparency in reporting. For further information on Nature Research policies, see Authors & Referees and the Editorial Policy Checklist.

Statistical parameters

When statistical analyses are reported, confirm that the following items are present in the relevant location (e.g. figure legend, table legend, main text, or Methods section).

n/a	Confirmed	
☐	☒	The exact sample size (*n*) for each experimental group/condition, given as a discrete number and unit of measurement
☐	☒	An indication of whether measurements were taken from distinct samples or whether the same sample was measured repeatedly
☐	☒	The statistical test(s) used AND whether they are one- or two-sided *Only common tests should be described solely by name; describe more complex techniques in the Methods section.*
☐	☒	A description of all covariates tested
☐	☒	A description of any assumptions or corrections, such as tests of normality and adjustment for multiple comparisons
☐	☒	A full description of the statistics including central tendency (e.g. means) or other basic estimates (e.g. regression coefficient) AND variation (e.g. standard deviation) or associated estimates of uncertainty (e.g. confidence intervals)
☐	☒	For null hypothesis testing, the test statistic (e.g. *F*, *t*, *r*) with confidence intervals, effect sizes, degrees of freedom and *P* value noted *Give P values as exact values whenever suitable.*
☒	☐	For Bayesian analysis, information on the choice of priors and Markov chain Monte Carlo settings
☐	☒	For hierarchical and complex designs, identification of the appropriate level for tests and full reporting of outcomes
☒	☐	Estimates of effect sizes (e.g. Cohen's *d*, Pearson's *r*), indicating how they were calculated
☐	☒	Clearly defined error bars *State explicitly what error bars represent (e.g. SD, SE, CI)*

Our web collection on statistics for biologists may be useful.

Software and code

Policy information about availability of computer code

Data collection	FACSDiva v8.0.1, StepOne v2.1. and 96.96 Dynamic Arrays with a BioMark system. For additional details please refer to Methods.
Data analysis	FlowJo v8.5.3; Prism v6.0; Excel v14.5.1; GSEA v3.0, GeneChip Operating Software, Bowtie version 0.12.8, TopHat version 1.3.2, Cufflinks version 2.0.2 and Hallmark version 6.2 for database. For additional details please refer to Methods.

For manuscripts utilizing custom algorithms or software that are central to the research but not yet described in published literature, software must be made available to editors/reviewers upon request. We strongly encourage code deposition in a community repository (e.g. GitHub). See the Nature Research guidelines for submitting code & software for further information.

Data

Policy information about availability of data

All manuscripts must include a data availability statement. This statement should provide the following information, where applicable:

- Accession codes, unique identifiers, or web links for publicly available datasets
- A list of figures that have associated raw data
- A description of any restrictions on data availability

All RNA-seq, microarray, and scRT-PCR data generated in this study are deposited in Gene Expression Omnibus (GEO) under accession code GSE122863. The data that support the findings of this study are available from the corresponding author upon reasonable request.

Field-specific reporting

Please select the best fit for your research. If you are not sure, read the appropriate sections before making your selection.

☒ Life sciences ☐ Behavioural & social sciences ☐ Ecological, evolutionary & environmental sciences

For a reference copy of the document with all sections, see nature.com/authors/policies/ReportingSummary-flat.pdf

Life sciences study design

All studies must disclose on these points even when the disclosure is negative.

Sample size	Sample size was chosen according to standard practices in the field.
Data exclusions	For single-cell qRT-PCR analysis, cells with undefined cycling threshold values (Ct= 999) for both gene = Gapdh and gene = Actb were excluded from our analyses.
Replication	We considered all of data were successfully reproduced by each attempt if similar results were obtained from at least 2 independent experiments.
Randomization	For in vivo experiments, mice of similar ages and sex were randomly used for all the experiments reported. In vitro experiments were all performed in parallel. Treatment wells were randomized in seahorse extracellular flux experiments to prevent variation due to micro-atmospheric conditions but otherwise we did not randomize in vitro experiments.
Blinding	The investigators were not blinded to the identities of the samples because treatments and data collection were performed by the same people. All samples were collected and analyzed at the same time under the same conditions. Blinding was not relevant for most in-vitro procedures as the readouts were automated and quantitative.

Reporting for specific materials, systems and methods

Materials & experimental systems

n/a	Involved in the study
☒	☐ Unique biological materials
☐	☒ Antibodies
☒	☐ Eukaryotic cell lines
☒	☐ Palaeontology
☐	☒ Animals and other organisms
☐	☒ Human research participants

Methods

n/a	Involved in the study
☒	☐ ChIP-seq
☐	☒ Flow cytometry
☒	☐ MRI-based neuroimaging

Antibodies

Antibodies used	The reagents used in this study were as follows: the FITC-, APC-, PE/Cy7-, BV421- and BV510-conjugated anti-CD4 (FITC; 100406, PE; 100408, APC; 100412, PE/Cy7; 100422, BV421; 100438, and BV510; 100449, GK1.5, 1 µg ml-1); PE-conjugated anti-CD8 (100708, 53-6.7, 1µg ml-1), PE-, APC-, and PE/Cy7-conjugated anti-CD62L (PE; 104408, APC; 104412, and PE/Cy7; 104418, MEL-14, 1µg ml-1); FITC- and PE-conjugated anti-CD44 (FITC; 103006, PE; 103024, IM7, 1 µg ml-1); FITC- and BV-421-conjugated Ly5.2 (FITC; 109806, BV421; 109382, 104, 1µg ml-1) and Ly5.1 (FITC; 110706, BV421; 110732, A20, 1µg ml-1); PE/Cy7-conjugated Thy1.2 (105326, 30-H12, 1µg ml-1) and Thy1.1 (202518, OX-7, 1µg ml-1); PE-conjugated anti-CCR7 (120106, 4B12, 1 µg ml-1), anti-GL7 (144608, GL7, 1µg ml-1), and anti-PD1 (135206, 29F.1A12, 1µg ml-1); and APC-conjugated anti-CD137 (106110, 17B5, 1 µg ml-1), and anti-KLRG1 (138412, 2F1/KLRG1, 1µg ml-1); Alexa647-conjugated anti-Foxp3 (126408, MF-14, 1µg ml-1); FITC-conjugated anti-CD11a (101106, M17/4, 1µg ml-1), anti-CD25 (101908, 3C7, 1µg ml-1), anti-CD27 (124208, LG.3A10, 1µg ml-1), anti-CD43 (121206, 1B11, 1µg ml-1), anti-122 (123208, TM-β1, 1µg ml-1), anti-CD127 (135008, A7R34, 1µg ml-1), anti-KJ1 (118506, KJ1-26, 1µg ml-1), anti-Fas (152606, SA367H8, 1µg ml-1); APC/cy7-conjugated anti-CXCR5 (145526, L138D7, 1µg ml-1), agonistic anti-CD28 (102102, 37.51, 1 µg ml-1), anti-IFNγ (505707, R4-6A2, 1µg ml-1) were purchased from BioLegend (San Diego, CA). Anti-IL-4 (554386, BVD4-1D11, 1 µg ml-1) was purchased from BD Biosciences. Alexa 488-conjugated anti-GPR34, anti-GIPR, and anti-TCF1 (#6444, C63D9, 1µg ml-1); Alexa 647-conjugated anti-pH2A.X (ser139)(9720, 20E3, 1 µg ml-1) were purchased from Cell Signaling. Agonistic anti-TCRβ (H57-597, 10 µg ml-1) was homemade.
Validation	Antibodies were chosen based on the validation statements for species (mouse) and application (FACS) on the manufacturer's website. For example, according to the manufacturer's website (https://www.biolegend.com/nl-nl/products/fitc-anti-mouse-cd4-antibody-248), the anti-CD4-FITC antibody was validated at least for the use of FACS analysis of mouse cells.

Animals and other organisms

Policy information about studies involving animals; ARRIVE guidelines recommended for reporting animal research

Laboratory animals	The animals used in this study were backcrossed to BALB/c or C57BL/6 mice 10 times. Acacafl/fl mice 1 were crossed with CD4-cre or ERT2-cre mice (Jackson Laboratory) and were maintained on a C57BL/6 background. OVA-specific TCR-αβ (DO11.10) transgenic (Tg) mice were provided by Dr. D. Loh (Washington University School of Medicine, St. Louis). Ly5.1 and Thy1.1 mice were purchased from Sankyo Laboratory. C57BL/6 mice and BALB/c mice were purchased from Clea Inc., Tokyo, Japan. The sex-matched mice were used at 7-14 weeks of age and maintained under specific-pathogen-free (SPF) conditions. The research proposals were reviewed by the ethics committee for animals atChiba University (registration number: 29-98, 29-99).
Wild animals	This study did not involve wild animals.
Field-collected samples	The study did not involve samples collected from the field.

Human research participants

Policy information about studies involving human research participants

Population characteristics	2 randomly selected healthy male and female donors
Recruitment	Blood from healthy donors was obtained from Chiba University, and used in compliance with Chiba University Administrative Panel for human subjects (authorization #1016). There was no selection bias.

Flow Cytometry

Plots

Confirm that:

☒ The axis labels state the marker and fluorochrome used (e.g. CD4-FITC).

☒ The axis scales are clearly visible. Include numbers along axes only for bottom left plot of group (a 'group' is an analysis of identical markers).

☒ All plots are contour plots with outliers or pseudocolor plots.

☒ A numerical value for number of cells or percentage (with statistics) is provided.

Methodology

Sample preparation	See Methods.
Instrument	Becton Dickinson 3-laser FacsCantoII for analysis and Aria III for cell sorting.
Software	BD FACSDiva software (BD Biosciences) for data acquisition and analyzed using FlowJo software v 8.5.3 (Tree Star). Data was graphed using Prism 6 (Graphpad).
Cell population abundance	The purities of sorted cell populations were consistently > 90-98%.
Gating strategy	The gating strategy is shown in each Figure.

☒ Tick this box to confirm that a figure exemplifying the gating strategy is provided in the Supplementary Information.